

Accepted Manuscript

Total dust deposition flux during precipitation in Toyama, Japan, in the spring of 2009: A sensitivity analysis with the NASA GEOS-5 Model

Tepei J. Yasunari, Peter R. Colarco, William K.M. Lau, Kazuo Osada, Mizuka Kido, Sarith P.P. Mahanama, Kyu-Myong Kim, Arlindo M. da Silva

PII: S0169-8095(15)00249-5
DOI: doi: [10.1016/j.atmosres.2015.08.005](https://doi.org/10.1016/j.atmosres.2015.08.005)
Reference: ATMOS 3474

To appear in: *Atmospheric Research*

Received date: 24 September 2014
Revised date: 4 August 2015
Accepted date: 4 August 2015



Please cite this article as: Yasunari, Tepei J., Colarco, Peter R., Lau, William K.M., Osada, Kazuo, Kido, Mizuka, Mahanama, Sarith P.P., Kim, Kyu-Myong, da Silva, Arlindo M., Total dust deposition flux during precipitation in Toyama, Japan, in the spring of 2009: A sensitivity analysis with the NASA GEOS-5 Model, *Atmospheric Research* (2015), doi: [10.1016/j.atmosres.2015.08.005](https://doi.org/10.1016/j.atmosres.2015.08.005)

This is a PDF file of an unedited manuscript that has been accepted for publication. As a service to our customers we are providing this early version of the manuscript. The manuscript will undergo copyediting, typesetting, and review of the resulting proof before it is published in its final form. Please note that during the production process errors may be discovered which could affect the content, and all legal disclaimers that apply to the journal pertain.

Total dust deposition flux during precipitation in Toyama, Japan, in the spring of 2009: A sensitivity analysis with the NASA GEOS-5 Model

Teppei J. Yasunari^{1,2,3}, Peter R. Colarco², William K. M. Lau^{2,4}, Kazuo Osada⁴, Mizuka Kido⁶,
Sarith P. P. Mahanama^{7,2}, Kyu-Myong Kim², and Arlindo M. da Silva²

¹*Goddard Earth Sciences and Technology and Research, Universities Space Research Association, Columbia, MD 21046, USA*

²*NASA Goddard Space Flight Center, Greenbelt, MD 20771, USA*

³*Now at Faculty of Engineering, Hokkaido University, Sapporo, 060-8628, Japan*

⁴*Earth System Science Interdisciplinary Center, University of Maryland, College Park MD 20740, USA*

⁵*Graduate School of Environmental Studies, Nagoya University, Nagoya 464-8601, Japan*

⁶*Toyama Prefectural Environmental Science Research Center, Imizu 939-0363, Japan*

⁷*Science Systems and Applications, Inc., Lanham, MD 20706, USA*

Corresponding author: Teppei J. Yasunari,

Faculty of Engineering, Hokkaido University, Sapporo, 060-8628, Japan.

E-mail: t.j.yasunari@eng.hokudai.ac.jp

Key words:

Dust; Wet deposition; Numerical modeling; Japan; Precipitation; Aerosol

ACCEPTED MANUSCRIPT

Highlight

- Total dust deposition flux during precipitation (TDP) at Toyama was evaluated with NASA GEOS-5.
- Four GEOS-5 experiments were analyzed to discuss the sensitivities on TDP for the two TDP events.
- Increased horizontal resolution increased modeled precipitation and TDP during the one event.
- One experiment (MERRAero) with aerosol data assimilation showed the best performance.
- A weak short-time precipitation during a dust transport event likely increased the observed TDP.

Abstract

We compared the observed total dust deposition fluxes during precipitation (TDP) mainly at Toyama in Japan during the period January – April 2009 with results available from four NASA GEOS-5 global model experiments. The modelled results were obtained from three previous experiments and carried out one experiment, which were all driven by assimilated meteorology and simulating aerosol distributions for the time period. We focus mainly on the observations of two distinct TDP events, which were reported in Osada et al. (2011), at Toyama, Japan, in February (Event B) and March 2009 (Event C). Although all of our GEOS-5 simulations captured aspects of the observed TDP, we found that our low horizontal spatial resolution control experiment performed generally the worst. The other three experiments were run at a higher spatial resolution, with the first differing only in that respect from the control, the second adding imposed a prescribed corrected precipitation product, and the final experiment adding as well assimilation of aerosol optical depth based on MODIS observations. During Event C, the increased horizontal resolution could increase TDP with precipitation increase. There was no significant improvement, however, due to the imposition of the corrected precipitation product. The simulation that incorporated aerosol data assimilation performed was by far the best for this event, but even so could only reproduce less than half of the observed TDP despite the significantly increased atmospheric dust mass concentrations. All three of the high spatial resolution experiments had higher simulated precipitation at Toyama than was observed and that in the lower resolution control run. During Event B, the aerosol data assimilation run did not perform appreciably better than the other higher resolution simulations, suggesting that upstream conditions (i.e., upstream cloudiness), or vertical or horizontal misplacement of the dust plume did not allow for significant improvement in the simulated aerosol distributions.

Furthermore, a detailed comparison of observed hourly precipitation and surface particulate mass concentration data suggests that the observed TDP during Event B was highly dependent on short periods of weak precipitation correlated with elevated dust surface concentrations, important details possibly not captured well in a current global model.

1. Introduction

Global climate models (GCMs), which incorporate coupled atmospheric and oceanic general circulation models (AGCMs and OGCMs, respectively, or AOGCMs when coupled), have been used to predict future climate (e.g., Emori et al., 1999; Hansen et al., 2007; Taylor et al., 2012). GCMs in either a forecast or hindcast mode have also been used to support field campaigns, where the data collected serves a crucial purpose in supporting model validation (e.g., Lawrence et al., 2003; Nowotnick et al., 2010, 2011a; Bian et al., 2013; Buchard et al., 2014). In terms of aerosol-related studies, most of the validation of GCMs has often focused on comparison of model variables to atmospheric observations from ground-based or satellite measurements (e.g., Takemura et al., 2000, 2002; Yu et al., 2003; Sanap et al., 2014). There has been far less focus on evaluating aerosol models in terms of simulated aerosol deposition due to the relatively sparse number of direct deposition measurements available (e.g., Ginoux et al., 2001; Luo et al., 2003; Mahowald et al., 1999, 2005, 2009; Inomata et al., 2009; Colarco et al., 2014a). As a result, aerosol deposition in global models is in general not well validated.

This paper focuses on evaluating the deposition of mineral dust aerosols during precipitation at Toyama, Japan, as simulated in the NASA Goddard Earth Observing System Model, Version 5 (GEOS-5) (e.g., Rienecker et al., 2008; Molod et al., 2012). For context, the phenomenon of the Trans-Pacific dust (or air mass) transport is well known (e.g., Duce et al., 1980; Shaw, 1980; Iwasaka et al., 1983; Darmenova et al., 2005; Yasunari et al., 2007; Yasunari and Yamazaki, 2009a, 2009b; Uno et al., 2009; Yumimoto et al., 2010; Yu et al., 2012; Yumimoto and Takemura, 2015). Because Japan sits on the Trans-Pacific air mass pathways, it is an ideal location to monitor Asian dust (also known as Kosa in Japanese), and dust transport has frequently been observed over Japan during springtime (e.g., Iwasaka et

al., 1983, 1988; Hao et al., 1995; Shimizu et al., 2004; Matoba et al., 2005; Kido et al., 2007; Hara et al., 2009; Mizoguchi et al., 2009) (also see the website on the general information on Kosa by the Japan Meteorological Agency, JMA, in Japanese: http://www.data.jma.go.jp/gmd/env/kosahp/kosa_data_index.html).

Osada et al. (2011; hereafter called OS11) have recently compiled weekly-resolved systematic measurements of the total dust deposition fluxes during precipitation (hereafter simply called, TDP; see Section 2.2) over a one-year period of time at six locations in Japan (Sapporo, Toyama, Tottori, Nagoya, Fukuoka, and Hedo) (their Fig. 1; Fig. 1). Yasunari et al. (2014; hereafter called, YS14) previously compared the modeled TDP from two global GEOS-5 simulations with the OS11 TDP observations at Sapporo in Japan to evaluate the sensitivity of the simulated snow darkening effect to the simulated aerosol deposition (the outputs from these two simulations were obtained and are also used in this study, focusing here mainly on the results at Toyama; see Section 2.1). Osada et al. (2014) recently extended the OS11 data by additionally including dry deposition data. Previous studies have shown that wet deposition plays a major role in the total dust deposition over the Pacific region (Uematsu et al., 1985) and the Japanese mountain range (Mount Tateyama in the Hida mountain range) (Osada et al., 2004). Therefore, we focus only on dust deposition during precipitation events in this paper using the OS11 TDP data set. Hereafter “observed TDP”, “TDP observations”, or similar descriptions for the observed TDP always refers to the TDP measurements by OS11.

In the spring of 2009, Asian dust transport to Toyama, Japan, during March 16-18 was reported by the JMA (Kosa-observed days and its locations in Japan in 2009; hereafter called, the JMA Kosa website 2009; available at the JMA website in Japanese:

http://www.data.jma.go.jp/gmd/env/kosahp/kosa_table_2009.html). During the same period, OS11 detected the two larger TDP events in the one of their six locations, Toyama (see Fig. 2 of OS11). They concluded that the greatest TDP event in March 2009 was due to the combined effect of precipitation and dust transport. Hence, we decided to mainly focus on the two TDP events at Toyama as good cases, during the time period of January – April, 2009, to evaluate GEOS-5 sensitivities and to further examine the observed TDP events.

The purpose of this paper is to compare experiments of GEOS-5 to observations made during the time period above in order to: (1) explore sensitivity of the modeled TDP at Toyama to model configuration characteristics; and (2) further understand why the OS11-observed TDPs from the events at Toyama were so pronounced. The outcomes of these investigations will enhance our confidence in the ability of chemical transport models to simulate dust deposition for real events, and suggest aspects of the modelling which require particular consideration because of the sensitivity of the simulated results (e.g., treatment of aerosol scavenging by precipitation).

2. Model setup and data set description

2.1 GEOS-5 model description and experimental design

GEOS-5 (Rienecker et al., 2008; Molod et al., 2012) is a global model for Earth system modeling developed by the NASA Global Modeling and Assimilation Office (GMAO; <http://gmao.gsfc.nasa.gov>), used for forecasting, data assimilation and reanalysis, and climate applications. Individual atmospheric, oceanic, and land surface components—including snowpack—are coupled under the Earth System Modeling Framework (Hill et al., 2004). GEOS-5 was used to produce the NASA Modern-Era

Retrospective analysis for Research and Applications (MERRA) atmospheric reanalysis product (Rienecker et al., 2011). A non-hydrostatic version of the GEOS-5 AGCM has been run at very fine horizontal resolution to simulate tropical cyclones and convective system (Putman and Suarez, 2011). In addition to traditional meteorological parameters, GEOS-5 simulates atmospheric aerosol components such as dust, sulfate, black carbon, organic carbon, and sea salt, using a version of the Goddard Chemistry, Aerosol, Radiation, and Transport (GOCART) module (Chin et al., 2000, 2002; Ginoux et al., 2001; Colarco et al., 2010). An aerosol data assimilation capability—used in one of our experiments below—has recently been introduced in GEOS-5, in which column-integrated total aerosol optical depth (AOD) derived from measurements made by the Moderate Resolution Imaging Spectroradiometer (MODIS) instruments on the NASA Terra and Aqua satellites is used to correct simulated total column aerosol optical depth (see details in Kessner et al., 2013; Buchard et al., 2014, 2015; Colarco et al., 2014b; Nowottnick et al., 2015). Additionally, YS14 (i.e., updated from Yasunari et al., 2011) recently developed a snow darkening module (called Goddard Snow Impurity Module: GOSWIM) as a part of the GEOS-5 land surface model, incorporating simulated deposition of dust, black carbon, and organic carbon aerosols from GOCART to snow in adjusting snow albedo physically. The impact of the snow darkening effect on boreal spring climate in the Earth system has recently been discussed with GEOS-5/GOSWIM (Yasunari et al., 2015). Evaluations of GEOS-5 aerosol simulations with field campaign and remote sensing data have been also presented in a number of recent studies (e.g., Colarco et al., 2010, 2014a,b; Nowottnick et al., 2010, 2011a; Bian et al., 2013; Buchard et al., 2014).

The GOCART module in GEOS-5 represents dust aerosols in five non-interacting size bins, covering the particle size range of 0.2-20 μm in diameter (Tegen and Lacis, 1996; Colarco et al., 2010). Dust

mobilization processes are based on Ginoux et al. (2001). As summarized in Nowottnick et al. (2011a), deposition processes include dry, wet (by convective and large-scale scavenging), and gravitational sedimentation. More detailed information on the dust treatment in GEOS-5 is also available in Colarco et al. (2010, 2014a) and Nowottnick et al. (2010, 2011a).

The dust wet removal schemes in GEOS-5 are primarily based on Liu et al. (2001). The wet removal process is separated into two types: wet scavenging (1) within convective plumes and (2) associated with large-scale cloud processes. The convective scavenging occurs in the cloudy fraction of the grid box with a rate proportional to the net convective updraft mass flux (updraft mass flux + entrainment - detrainment). The rate is scaled by an overall scavenging efficiency, which is determined by the updraft velocity speed (assumed to be 5 m s^{-1} over water and 10 m s^{-1} over land) and the height of the convective plume. The large-scale in-cloud scavenging is proportional to the grid box fraction of the precipitating cloud and is scaled by the precipitation rate. The below-cloud washout follows a similar formulation but accounts for tracer return via evaporation if precipitation in the grid box is less than precipitation in higher grid boxes. For dust, an efficiency factor of 0.3 is assumed for in-cloud scavenging to account for the reduced hygroscopicity of dust relative to other aerosols. The column accumulated wet removal amount for each case is the total wet deposition amounts at each grid point by convective and large-scale scavenging, respectively.

The results from four GEOS-5 experiments (EXP1-4; see below) were used in this study. For all simulations, the model had 72 vertical hybrid sigma levels, which is a typical GEOS-5 configuration (Rienecker et al., 2008; Molod et al., 2012), extending from the surface to approximately 85 km altitude. We explore two different horizontal spatial resolutions ($2^\circ \times 2.5^\circ$ and $0.5^\circ \times 0.625^\circ$ latitude by longitude) in

order to investigate sensitivity of simulated aerosol emission, transport, and deposition, as well as simulated precipitation, to spatial resolution. Nowottnick et al. (2011b) found that spatial resolution had a significant effect on the magnitude of dust emissions in GEOS-5 because higher resolution versions of the model had typically higher surface wind speeds. Additionally, Toyama—where we focus in this study—is located in the vicinity of the Hida mountain range, so we expect some sensitivity on changing spatial resolution due to sharp gradients in topography though other factors are also possible. All of our experiments are “replay” simulations, in which the GEOS-5 produced MERRA atmospheric reanalysis fields (pressure thickness, virtual temperature, horizontal winds, ozone, and specific humidity) by Rienecker et al. (2011) are used to replace the atmospheric state every six hours of simulation time to the MERRA reanalysis fields, and the full model physics is used to simulate the atmospheric state for subsequent time steps until the next analysis update is available (also see, for example, Supplemental Information, SI, of YS14). As summarized in Nowottnick et al. (2011a), this cycling strategy allows GEOS-5 to reproduce observed meteorology similar to what is typically done for offline chemical transport models, but without the expense of running the atmospheric data assimilation system at the same time. For all experiments, the observation-based sea surface temperature data set of Reynolds et al. (2002) was prescribed as a surface boundary condition.

The four GEOS-5 experiments used in this study are:

EXP1: This experiment is identical to the TE1 experiment presented in YS14 and the outputs were obtained from their study. This experiment was performed at 2° (latitude) x 2.5° (longitude) horizontal resolution (144 x 91 grid points in longitude by latitude) and the precipitation was generated by the model.

The EXP1 simulation started from June 18, 2004 (YS14).

EXP2: This experiment is identical to the TE2 experiment also presented in YS14 and the outputs were obtained from their study. It is similar to EXP1 discussed above except that the experiment is performed at 0.5° (latitude) x 0.625° (longitude) horizontal resolution (576 x 361 grid points in longitude by latitude.) and started from May 23, 2008 (YS14). The model also simulated the precipitation, as similarly does in EXP1.

EXP3: This experiment is similar to EXP2 (0.5° x 0.625° horizontal resolution), but instead of only generating the precipitation by the model as in EXP1 and EXP2, this experiment further used a forcing of the corrected 1-hourly precipitation product (Reichle and Liu, 2014; hereafter referred to as the corrected MERRA precipitation), using the global precipitation products based on observations and estimates from satellite data (Adler et al., 2003; Xie et al., 2007) to replace the simulated precipitation. EXP3 also began on May 23, 2008. This experiment was carried out for this study.

EXP4: This experiment's results were obtained from the recently produced "MERRAero" aerosol reanalysis, in which aerosol optical depth was assimilated from a MODIS-derived AOD product (see below). This experiment was also carried out at 0.5° x 0.625° horizontal resolution and used the corrected MERRA precipitation product. See Kessner et al. (2013), Buchard et al. (2014, 2015), Colarco et al. (2014b), and Nowottnick et al. (2015) for further information about MERRAero.

We note that EXP1-3 were all carried out with identical versions of the GEOS-5 model code, which incorporated the snow darkening effect by YS14 in the land surface model. EXP4 was carried out with a slightly different version of the model that neglected, for example, the snow darkening effect. This difference, and other differences in the model codes between EXP4 and the other experiments are insignificant to our results on the replay run experiments, for which all the experiments are constrained by

the MERRA atmospheric reanalysis fields (Rienecker et al., 2011). We mostly used the GEOS-5 outputs during January – April 2009 except for Figs. S2 and 9.

For comparisons to observations, the TDP is computed from the GEOS-5 outputs as in YS14 as the weighted sum of dust sedimentation and dry and wet deposition fluxes during the simulated precipitation event (defined here as in YS14 as a total precipitation rate—including convective and large-scale rain and snowfall—in excess of $1.0\text{E-}20$ mm day⁻¹) with the particle size weighted treatment as follows. As inherited from the previous studies (Tegen and Lacis, 1996; Colarco et al., 2010), the dust particle size distribution is resolved into five size bins, for which each bin has an assumed sub-bin particle size distribution used for calculating its optical properties. The smallest of these size bins spans a diameter range of 0.2 – 2 μm . Because OS11 used filters with 1.0 μm sized pores for the TDP measurement (see Section 2.2), in order to make better comparisons of TDP between the OS11 observations and models in closer particles size ranges, we accordingly aggregate dust mass fluxes from the model as the total of 67.6% of the flux in the smallest size bin (i.e., corresponding to the sub-bin particle diameter size range of 1.2 – 2 μm) and the fluxes in our four larger size bins for the purpose of data analyses. So as to avoid arbitrary settings, we followed the mass fraction settings above based on the previous studies (Tegen and Lacis, 1996; Colarco et al., 2010). This treatment was applied to all the dust deposition components (sedimentation, dry, and wet deposition fluxes) from the GEOS-5 outputs, which is also applied to compute modeled dust emission flux for our discussion.

For simulated mass concentration and column mass density of dust, the saved variables were not separated into the particle size bins in the original GEOS-5 settings, reflecting all size information and are compared as they are to the available atmospheric observations (see Section 2.2). If we need to discuss in

detail the mass concentration and column mass density in separated dust size bins, we have to change the GEOS-5 output settings in future studies. However, the sub-bin mass separation for the smallest size bin, which was carried out for the modeled TDP, is not necessary especially for the comparison between modeled surface mass concentration of dust and observed (and/or estimated) Total Suspended Particles (TSP) (see Section 2.2 and Section 3 of Supplementary Information, SI) because TSP includes all particle sizes. The additional information on the treatment of the GEOS-5 data is also available in SI.

2.2. Observations in Toyama

We compare the GEOS-5 simulated TDP to observations made in Toyama, Japan, by OS11. Note that OS11 call their measurements the “wet deposition flux” of dust, but strictly it is the sum of all the possible components of dust fluxes captured (by dry and wet processes) during precipitation events, as discussed in YS14. Here we summarize the measurement approach used in OS11. Briefly, their measurement system employed a precipitation sensor that opened the sampler when precipitation was detected. They filtered the collected water sample including deposited materials with 1.0 μm sized pores. The sampling interval of OS11 was mostly weekly, with some exceptions, at which point the sample bottles were changed and the next sampling period began. They estimated the dust amount from the measured iron (Fe) mass in the insoluble residue collected on the filter, using the method of Ura et al. (2011), in which the total mineral dust mass was assumed to include 3.8% Fe by weight (see more information in OS11).

The OS11 TDP observations were taken at six locations in Japan (Sapporo: 43.08°N, 141.34°E; Toyama: 36.70°N, 137.19°E; Nagoya: 35.16°N, 136.97°E; Tottori: 35.54°N, 134.21°E; Fukuoka: 33.55°N, 130.36°E; Cape Hedo; 26.86°N, 128.25°E) (Fig. 1 of OS11; Fig. 1). As mentioned, in this paper we focus

primarily on the measurements at Toyama, mainly using the observed TDP data there to evaluate the calculated TDP from the GEOS-5 simulations. We also use the observed TDP data at the other locations in Section 3 to give some broader context to our comparisons.

The Japan Meteorological Agency (JMA) observed the precipitation data using the Automated Meteorological Data Acquisition System (AMeDAS; see the JMA website in Japanese at: <http://www.jma.go.jp/jma/kishou/known/amedas/kaisetsu.html>), which we use here for the comparison with the GEOS-5 results and other datasets in order to present the timing and amount of precipitation observed and its possible impact on the observed TDP. The JMA station location information (the location information available in degrees and minutes) and daily precipitation data (also hourly precipitation data for the purpose of the discussion in Section 3.3) were obtained from the following JMA website (in Japanese) (available at: <http://www.data.jma.go.jp/obd/stats/etrn/index.php>). For our discussion, we chose the JMA Toyama station (36.7°N, 137.2°E), which is nearby to the location where the TDP observation at Toyama was made.

There were additionally ground-based lidar data available in Toyama prefecture from a part of the lidar network maintained by the National Institute for Environmental Studies (NIES) (Sugimoto et al., 2008). These data were used to investigate the timing and altitude of dust transport to Toyama. The NIES lidar is located at the Toyama Prefectural Environmental Science Research Center (TESC; 36.70°N; 137.10°E) in Imizu city, which is very close to the TDP observation site in Toyama city (approximately 8 km away, which was calculated on Google Earth). The lidar data are available from the NIES website (available at: <http://www-lidar.nies.go.jp/>). Here, the attenuated backscatter coefficient (ABC) and depolarization ratio (DR) at 532 nm were used. We follow the recommended data treatment given to us by

NIES (Shimizu, A., and N. Sugimoto, personal communication, 2012): We ignore data for $ABC < 0.4 \text{ Mm}^{-1} \text{ sr}^{-1}$ (i.e., the data were considered to be below confident detection thresholds) and assume that instances of $ABC > 10.0 \text{ Mm}^{-1} \text{ Sr}^{-1}$ are generally indicative of clouds rather than aerosols (Shimizu, A., and N. Sugimoto, personal communication, 2013). Additionally, DR is well known as a good indicator of non-spherical particles (i.e., ice crystals and dust particles, e.g., Iwasaka, 1986a, 1986b; Iwasaka et al., 1988). As mentioned in Shimizu et al. (2004), the histogram of the NIES lidar in-cloud DR data shows two peaks, possibly identifying water (around a few percent) and ice (30%) clouds. Based on their criteria, DR values of roughly 10-20% with corresponding enhanced ABC values (but smaller than the $10.0 \text{ Mm}^{-1} \text{ Sr}^{-1}$ threshold noted above) are attributed to the occurrence of mineral dust.

We also used Suspended Particulate Matter (SPM) data, which were measured (by the β -ray absorption method), maintained, and provided by the TESC. We used the SPM data to understand the surface air quality in Toyama city. The SPM measurement includes only aerosol particles of $< 10 \mu\text{m}$ in diameter (e.g., Fig. 14 of Kasahara, 2002). Hao et al. (1995) mentioned that SPM measurement based on the β -ray absorption method made it possible to distinguish Asian dust (Kosa) events, but the measurement based on light scattering did not. Hence, the SPM observations at TESC by the β -ray absorption method could be suitable to discuss Asian dust events. The calculated daily mean SPM data was based on the 1-hourly observed data and then averaged in 9 locations in Toyama city (the location information was provided by TESC; Table S1). The averaged data are regarded as representative of the SPM concentration in Toyama city. See more information on the SPM data in Section 2 of SI.

Total Suspended Particles (TSP) measurements were also used to evaluate the total pollution level (i.e., the SPM is limited to particle sizes of $< 10 \mu\text{m}$ diameter, as mentioned above, but the TSP data

includes all particle sizes). The TSP measurement method was based on Kido et al. (2007), for which the weights on filtered samples were measured to obtain the mass concentrations. The TSP observations were only sporadically carried out at TESC during March-April 2009, including measurements during both Kosa (Asian dust) and non-Kosa conditions (Table S2), but unfortunately did not fully cover the time period of this study (January – April 2009). To make it possible to compare TSP with other data, we calculated an “estimated” TSP, using the SPM data with the relationship between the SPM and TSP data during the limited time period of coincident coverage (see Section 3 of SI). The information on the difference between the SPM and TSP measurements can provide us the mass information from atmospheric pollution contributed by the particles of larger than 10 μm diameter.

2.3. Temporal re-sampling of data

Because of the different time intervals, when we directly compare our modelled results (i.e., daily data) from GEOS-5 (or other observed quantities) to the observed OS11 TDP (i.e. mostly about weekly mean flux data), we have to temporally re-sample the quantities to the observed TDP sampling time intervals. Based on the YS14 method, we applied their temporal re-sampling method to the daily data here. For calculating temporally re-sampled mean modeled TDP, the modeled daily quantities were summed up with weighted fractions of each day (i.e., sum of the products of the daily quantity and fraction) during each sampling time period of the TDP observations (i.e., if the one modeled daily quantity on a certain day was completely within the time range of the one observed TDP sample, the day fraction for the daily data on that day is 1.0; if the modeled daily quantity on a specific day was partially overlapped with the time period on that day of an observed weekly TDP sample (this may happen mostly for the start and/or end

days of each sampling time interval of the TDP observation), the day fraction was smaller than 1.0, depending on its overlapped time). To obtain each time-interval mean TDP, we divided the accumulated quantities (i.e., the sum of the product above) by each OS11 sampling time interval of the observed TDP. Then we can directly compare the temporally re-sampled mean modelled TDP to the observed TDP in its time intervals (i.e., temporally consistent mean flux data).

For temporally re-sampled mean modelled surface mass concentration of modeled dust, the re-samplings were also similarly calculated, but the division was carried out by the accumulated day fraction within the available data during each observed TDP sampling time interval. However, there were no missing data in the modelled outputs on the surface mass concentration and the method was the same as the TDP re-sampling calculation above. The re-sampled mean data are considered as the mean data for each observed TDP sampling time interval.

The JMA-observed and GEOS-5-modeled daily precipitation rate data were also temporally re-sampled so as to have the observed TDP sampling time intervals. For the purpose of the discussion in Section 3 of SI, we also temporally re-sampled the simulated surface mass concentrations of dust to the sampling time intervals of the observed TSP (Table S2). The areal averaged daily mean SPM data in Toyama city (nine locations) are also temporally re-sampled so as to have the same sampling time intervals of the observed TDP or TSP (see Section 3 of SI).

3. Two observed TDP events at Toyama in the spring of 2009

Fig. 2 shows the detailed comparisons of the modeled GEOS-5 results to observed TDP, surface-level aerosol mass concentration (the observed SPM, modeled dust, and estimated TSP), and precipitation

(from the JMA observations) at Toyama during the period January – April 2009. The “estimated” TSP for comparisons with GEOS-5 outputs was computed, which was based on the temporally re-sampled SPM data in Fig. 2b with the non-linear regression equation (Eq. 2) from the relationship between SPM and TSP shown in Fig. S3a (also see Section 2.2 and SI). As summarized in Section 2.3 and SI, all the data in Fig. 2 except for the observed TDP and estimated TSP were temporally re-sampled to the observed OS11 TDP sampling time intervals.

During the January – April 2009 time period OS11 reported two distinct TDP events in Toyama: one in late February (their Event B, spanning the time interval 13:15 Japan Standard Time (JST) February 18 and 15:45 JST February 25) and one in Mid-March (their Event C, from 12:20 JST March 11 to 12:35 JST March 18) (Fig. 2a). All of the GEOS-5 simulations showed at least somewhat the increased TDP during Events B and C (Fig. 2a), with model performance varying among our four experiments, especially for Event C. In the remainder of the paper we seek to understand this diversity in the simulated results.

3.1 Impact of increasing model horizontal resolution on the simulated dust characteristics from near the dust source region to Japan

We first seek to understand the role of model spatial resolution as it related to the dust emission and transport characteristics from the dust source regions to Japan during the January – April 2009 period. Here we particularly investigate EXP1 and EXP2 (i.e., only the horizontal resolutions were different). We note that overall at Toyama both the seasonally accumulated TDPs in EXP1 and EXP2 underestimated the observed TDP (Table 1). In detail, we see much higher TDP in the higher resolution EXP2 simulation.

We first considered that one possible explanation for the different TDP from these two simulations lies simply in the amount of dust present in the atmosphere, and that this is controlled to first order by the dust emission process. Fig. 3 shows the accumulated dust emission fluxes for both EXP1 and EXP2 over the January – April 2009 period, showing particularly the main sources of dust from the Taklamakan and Gobi desert regions. Dust emissions in GEOS-5 are strongly controlled by surface wind speed (i.e., an approximately cubic dependence on wind speed, see Nowottnick et al. 2010), parameterized here in terms of the 10-m wind speed (Ginoux et al., 2001). Superimposed on Fig. 3 are the mean 10-m surface wind speeds for both simulations, which are clearly stronger (weaker) in EXP2 (EXP1), leading to higher (lower) dust emissions. The result is similar to what was found by Nowottnick et al. (2011b) in their simulations with GEOS-5. These suggest us that in general coarser topography may generate weaker horizontal gradient on its topography resulting in lower wind speeds. The major dust source in the Taklamakan Desert in EXP1 (i.e., the area with the relative increases of dust emission at the left side in Fig. 3) is at relatively lower altitudes than steep mountainous terrains on its southern border (see Fig. S1), and high spatial resolution simulation (EXP2) suggests much of the dust emission in this region is driven by stronger surface winds at the southern border, as similarly discussed in Nowottnick et al. (2011b). We note that for both spatial resolutions the underlying dataset of topography is the same, but at the coarser resolution the “peaks” and “valleys” in the topography are relatively smoother. The enhanced surface wind speeds apparent in the higher resolution EXP2 were seen around the areas with the strong altitude gradients, and these gradients were more pronounced in the EXP2 run (Fig. S1). However, higher wind speeds were also seen in the EXP2 run in regions with gentler topographic gradients, so the generally higher dust emissions in EXP2 are perhaps driven by some combination of topographically driven winds

and other possible factors. This discussion does not preclude, however, other possible contributions to the increased dust emissions, such as differences in soil moisture, which can reduce dust emissions in wetter areas. Further model simulations are needed to understand the spatially dependent processes governing the dust emissions in this region.

Calculating the sum of the accumulated amount of dust emissions over the whole domain in Fig. 3 during the January – April 2009 period (see the related information in SI), we obtained domain-integrated (i.e., the domain of Fig. 3) total dust emissions of about 17.6 and 32.7 Tg for EXP1 and EXP2, respectively (i.e., emissions in EXP2 are nearly twice as great as in EXP1).

However, interestingly, the increases in dust emissions in the source regions associated with increased model horizontal resolution did not necessarily imply increased TDP at the target location, Toyama (Fig. 2a; Table 1). Even though the emission increased around the Taklamakan and Gobi deserts as horizontal resolution increased (Fig. 3), the resultant column mass densities of dust over Japan between EXP1 and EXP2 had smaller differences (Fig. 4). This is probably attributable to the larger mass loss of dust near the source regions and during transport to Japan (i.e., more emission in EXP2 as seen in Fig. 3, but also more deposition near the source region as seen for the TDP plots shown in Fig. 5). Hence, the increased TDP in EXP2 at Toyama (Fig. 2a, Table 1) should be mainly affected by other possible factors.

A possible explanation for the modelled TDP increase at Toyama between EXP1 and EXP2 (Fig. 2a; Table 1) is that, as illustrated in Fig. 2c and Table 2, there is simply more precipitation simulated at Toyama in EXP2 than that in EXP1. The large-scale dynamical forcing in these two simulations are similar (i.e., both simulations are driven by the same meteorological reanalysis fields) and in this version of GEOS-5 there are no aerosol indirect effects, as similarly mentioned in Randles et al. (2013). So

differences in aerosol loading would only affect precipitation through the presumably weak aerosol direct radiative effect (recall, the dynamical forcing is reset to the MERRA analysis fields every six hours). There is clearly some dependency of the simulated precipitation then on the model spatial resolution. Accordingly we speculate that these differences may result from the differently resolved representation of topography near Toyama. Chao (2012) points out a long standing problem for GCMs in that they typically overestimate precipitation in the presence of steep terrain as a result of not properly ventilating heat from the boundary layer during the daytime on upslope faces of mountainous terrain. Chao (2012) and Chao (2015) suggest a parametric resolution to this problem for GCMs, but it has not been applied in our version of GEOS-5. As Figure 2c shows, the integrated precipitation at Toyama during Events B and C in the higher spatial resolution is generally overestimated by GEOS-5, and the overestimate is also seen in the seasonally accumulated precipitation (Table 2), which may be somewhat explained by Chao (2012) and Chao (2015).

Fig. 6 shows an east-west cross section of how the surface topography, specific humidity, vertical wind speed, and dust concentrations differ at the latitude of Toyama in the two simulations (EXP1 and EXP2) on March 16, 2009 during Event C. Toyama is situated near the coast, with water to the west and the Hida Mountains immediately to the east, and it is apparent in Fig. 6 that the resolved surface structure in the model has a steeper gradient and correspondingly larger vertical wind speeds in the EXP2 model run. These results are consistent with the explanation for excessive precipitation offered by Chao (2012). As seen in the surface geopotential height in Fig. 1, the steepest terrain gradients were seen around Toyama in Japan in EXP2, compared to EXP1. Furthermore, we found that the largest increase in modelled TDP when increased the horizontal resolution was seen during Event C at Toyama within the six OS11

measurement sites (Fig. S2). Although we have discussed the horizontal characteristics thus far, we will discuss in detail GEOS-5 model sensitivities on TDP for Event B and C, compared to observations, in the following sections.

3.2 A strong Asian dust event at Toyama in March 2009 (Event C)

The correlated rise in the observed TDP and aerosol surface mass concentration (SPM) is more clearly pronounced for Event C than for Event B (Fig. 2a,b; see also the much clearer increase in the daily mean SPM data in Fig. S4). Event C again represents the greatest observed TDP in the OS11 data set (Fig. 2 of OS11; Fig. S2). The JMA officially observed Asian dust, Kosa, at Toyama during this time period (March 16-18) (see the JMA Kosa website 2009). On March 16-17, additionally, here the NIES lidar observations in Toyama prefecture of both the attenuated backscatter coefficient (ABC; Fig. 7a) and depolarization ratio (DR; Fig. 7b) at 532 nm are strongly indicative of increased atmospheric dust (also see Section 2.2 for the interpretation of the lidar data), as also discussed in OS11 (see their Fig. 4). Finally, the suite of GEOS-5 simulations also more clearly captured the features of Event C than Event B (e.g., Fig. 2).

There are large differences in the simulated precipitation rates during Event C for EXP1 and EXP2 (Fig. 7d,e). The JMA observed daily precipitation rates at Toyama are 0.5 and 6.0 mm day⁻¹ on March 16 and 17 (total 6.5 mm; total 3.5 mm during the exact one-day time period on March 16 in EXP1-3), respectively, while the simulated daily precipitation amount on March 16 was smaller for EXP1 (1.8 mm) and larger for EXP2 (11.6 mm). The precipitation amounts on that day in EXP3 (12.1 mm) and EXP4 (15.8 mm; one-day time period is slightly different from those in EXP1-3 as in Section 1 of SI) were similar to that of EXP2. The precipitation in GEOS-5 on March 16 is critical for the increased TDP, as this

is when the peak in the dust transport occurred over Toyama (Fig. 7). The vertical profile of the dust mass concentration was similar in EXP1 and EXP2 (Figs. 6 and 7d,e). The precipitation during Event C coincided with higher specific humidity (Fig. 6) in the lower troposphere, overlapping the altitude of the dust layers. So we considered that the increased specific humidity might contribute to the increased precipitation in the dust layers and then might be presumably responsible for increasing the TDP amount at the surface. In EXP1, the mountain range near Toyama was resolved only as plateau-like wide and flat feature near the surface (the white masking in Fig. 6; see also Fig. 1). The enhancement of these meteorological features with the increased horizontal resolution in EXP2 is probably relevant to increased precipitation amounts at the surface (Fig. 7d). We speculated above that this enhanced precipitation in EXP2 relative to EXP1 results from the simulated greater upward motion of the air brought on by the more sharply resolved surface structure in EXP2 (i.e., topography effect). However, we cannot exclude other contributions too in addition to above within currently what we have. Therefore, we cannot firmly conclude this point in this study and further investigations are needed in future studies.

EXP3 used the corrected MERRA precipitation rather than modeled precipitation (as in EXP2), but at Toyama there was very little difference in the precipitation during Event C when EXP3 and EXP2 are compared (Fig. 2c). The TDP difference during Event C was small (slightly less TDP in EXP3 than that of EXP2, Fig. 2a).

The greatest increase of TDP was obviously seen for EXP4 (Fig. 2a). Recall that EXP4 was like EXP2 except now with both the inclusion of the corrected MERRA precipitation (as in EXP3) and aerosol data assimilation. We note that the assimilation of aerosol information happens not only at the local level but also at upwind regions. The result is that EXP4 showed a higher mass concentration of dust in the lower

troposphere near Toyama compared to EXP1 and EXP2 (Fig. 7c-e). Comparisons of day-to-day atmospheric dust transport between EXP3 and EXP4, for example, clearly showed how the aerosol data assimilation increased the atmospheric column mass density of dust during the time period of March 14-16, 2009 (Fig. S5). On March 14, atmospheric dust was high around the Gobi desert region in both EXP3 and EXP4, indicating an Asian dust outbreak there, and the atmospheric dust amounts between these experiments were almost the same. It is not until March 15 that the benefit of the MODIS aerosol observations were realized in the model, at which point the data assimilation introduced a significant correction to the aerosol loading over the East China Sea between Beijing and the Korean Peninsula, and the atmospheric dust amount in EXP4 was dramatically increased, compared to what was found in EXP3. This continued on March 16, by which point the aerosol plume had reached Japan. The maximal column densities of dust in EXP4 on March 15 and 16 were a factor of 2.5 and about 1.8 greater than those in EXP3 in the East Asian domain, respectively (Fig. S5). The aerosol data assimilation in this case resulted in significantly increased atmospheric mass concentration of dust near Toyama, as seen in the vertical profile from the surface to the free troposphere levels on March 16 for Event C (Fig. 7c). The simulated daily mean surface mass concentration of dust in EXP4 was closer to the estimated TSP (estimated Total Suspended Particulate level at surface) in Fig. S4 (see also the TSP estimate from the temporally re-sampled SPM data in Fig. 2b). The comparison indicated that EXP4 more reasonably captured the observed surface pollution level caused by the Asian dust transport. Because we showed previously that use of the corrected MERRA precipitation had minimal effect for this event (and in any case the simulated precipitation rates in EXP2-4 were somewhat higher than observed), we conclude that the improvement of TDP in EXP4 (Fig. 2a) can be attributed mainly to the significant increase of atmospheric dust by the

aerosol data assimilation (Figs. S5 and 7), with the deposition scaled accordingly given the similar degrees of precipitation in EXP2, EXP3, and EXP4. Despite this improvement, more than half of the observed TDP for Event C could not be explained by EXP4 (Fig. 2a).

To summarize our simulations of Event C, we found similar atmospheric dust loadings over Toyama in EXP1-3, while EXP2-4 had similar precipitation as follows. EXP1 had less precipitation on March 16 during the event as compared to the JMA observations. Then, the precipitation in EXP2 was somewhat higher than the JMA-observed one, but was similar to the ones with the MERRA-corrected precipitation used in EXP3-4. The greater precipitation in EXP2-3 resulted in greater TDP than was found for EXP1. The largest amount of modeled TDP for Event C was found in EXP4, where the aerosol data assimilation process had significantly enhanced the dust loading. Even so EXP4, which captured the estimated TSP quite well, could only explain less than half of the observed TDP, suggesting even higher dust loading at elevated altitudes would have been needed or else that some aspect of the dust-precipitation interaction is not adequately simulated in the model (either the vertical position of the dust and precipitation, or else possibly in the aerosol particle sizes and/or the wet removal process parameterization itself, such as the scavenging efficiency). We have additionally speculated that the major difference in the simulated precipitation between EXP1 and EXP2 is critically dependent on how topography was resolved. A recent regional modelling study by Uno et al. (2014) found that topography (i.e., altitude) effect was critical in simulating the precipitation (i.e., snow) distributions in a nearby region of Toyama prefecture in Japan, further supporting our speculation of the role of orographic forcing in governing the precipitation in Toyama. Chao (2012), on the other hand, points out that GCMs typically simulate excessive precipitation in the vicinity of steep terrain, which would be exacerbated in our higher resolution simulations, and

indeed the precipitation at Toyama was overestimated in EXP2-4. Unfortunately, with our current experiments cannot conclusively implicate the topography effect as an explanation for the precipitation increase in those simulations, and in any case EXP3-4 were using a corrected precipitation product which itself did not agree with the observations taken in Toyama. Hence, this would be a good motivation for a future study to obtain more conclusive results on the topography-precipitation relationship.

3.3. A weak dust event at Toyama in February 2009 (Event B)

Event B is characterized by about 37% value of the observed TDP for Event C (Fig. 2a). The temporally resampled SPM (or estimated TSP) data show lower pollution levels during Event B compared to Event C (Fig. 2b), although the higher time resolution NIES lidar data clearly show the amplified signals implying enhanced surface dust concentrations at the TESC site on February 21 (Fig. 7a,b; different plots of ABC and DR with the same NIES lidar data in Toyama during February 18-22 were also available at the NIES lidar website at: <http://www-lidar.nies.go.jp/Toyama/archives/090218-090222.png>, hereafter called the NIES lidar-plot 090218-090222 website). The daily mean observed SPM and estimated TSP data also show relative increases in the pollution levels on February 21 compared to the surrounding days (Fig. S4). On the other hand, the JMA-observed daily precipitation rate at Toyama on February 21 was just 1.0 mm day^{-1} (Fig. 8), and JMA did not officially report Asian dust events at Toyama at all in February, although Asian dust events were reported in other prefectures (mostly in the western part of Japan) around February 20-22 (see the JMA Kosa website 2009). A trajectory analysis based on the HYSPLIT model (Draxler and Rolph, 2014; Rolph, 2014; see the website at: <http://ready.arl.noaa.gov>) suggests that low altitude air masses had their origins over the Gobi desert region on the preceding days,

suggesting the possibility of Gobi dust as the contributor to the dust loading of Toyama during this event (see Section 4 of SI and Fig. S6).

While for Event C we found that the four model simulations had very different TDP from one to another, for Event B the TDPs in the higher resolution simulations (EXP2-4) have essentially the same, about twice as great as was found for the lower resolution EXP1 simulation (Fig 2a). The simulated surface mass concentrations of dust were similar for all of the model simulations (Fig 2b). The similarities in the different simulations' surface mass concentrations of dust can be more clearly seen by looking at the daily data (Fig. S4). The enhancements in the simulated surface mass concentrations of dust were weak on and around February 21 for all the experiments here (Fig. S4). Comparing Fig. 7e (EXP1) with Fig. 7c,d (EXP4 and EXP2, respectively) shows some difference in the vertical profile of the dust loading simulated in the lower resolution EXP1 simulation. The JMA observation showed very weak precipitation rate of 1.0 mm day^{-1} on February 21 (Figs. 8 and S4) and did mostly no precipitation during the exact covered-time of the daily data in EXP1-3 (after 6:00 JST in Fig. 8 and partially not shown on February 22). The model precipitation is very weak on February 21 (Fig. 7c-e), but precipitation is somewhat higher on surrounding days and for the entire TDP aggregating period we find the modelled precipitation is actually somewhat higher than what was observed (Fig. 2c). Interestingly, EXP4 with the assimilation of aerosol data did not result in a significantly better simulation of this event (Figs. 2b and S4), possibly either because cloudiness over Toyama or at upwind locations prevented successful MODIS aerosol retrievals to assimilate, or possibly because the aerosol plume was misplaced in altitude or horizontal position in the model, which would not be corrected by the assimilation methodology (i.e., there is no vertical information in the MODIS observations). The lower altitude dust concentrations simulated (Fig. 7c-e) are somewhat similar

to the “background Kosa” (pg. 494) condition typically seen in the free troposphere with regard to weak dust concentrations of about $0.0019\text{--}0.025\text{ mg m}^{-3}$ as in Iwasaka et al. (1988). This is also consistent with the discussion on the weak Asian dust transport from the observations with the trajectory analysis in the last paragraph and Section 4 of SI. Overall, the reproducibility of observed TDP for Event B by the simulations was poor in terms of magnitude, compared to that of Event C.

Although the modeled TDP showed less increases in the four experiments during Event B, the observed TDP did a significant increase (Fig. 2a). Then, we must ask us, “What is the reason why the observed TDP in Fig. 2a could greatly increase during Event B?” To investigate the reason, we further examine the observed 1-hourly SPM data (averaged the nine-location data excluding missing data) and JMA-observed precipitation data during the time period covering Event B (Fig. 8). Fig. 8 breaks down the almost one TDP sampling period into hourly data spanning the period February 18-25, which encompasses the observed TDP sampling period for Event B (from 13:15 JST February 18 to 15:45 JST February 25). Over most of this period the SPM was low, which seemed to be near background levels. The enhancements occurred over the evening hours on February 20 and the early morning hours on February 21. On February 20 there was precipitation of 1.5 mm h^{-1} during 18:00-19:00 JST, near the beginning of the enhancement in the observed SPM, but there was no precipitation during the peak SPM values later that evening. This suggests that most of the dust during the evening hours were not washed out by precipitation (i.e., small impact on the observed TDP). The SPM values peak again in the early morning on February 21, during which time the precipitation was very weak (0.5 mm h^{-1}) but steady for two hours between 2:00 and 4:00 JST. The relationship between the increased precipitation and SPM on February 20-21 may be the typical pattern of a cold front system, which generates precipitation first, followed by

dust transport (i.e., high dust concentration backward of the cold front) (e.g., see Fig. 4 of Sugimoto et al., 2003; Fig. 3 of OS11). Based on the results on February 20 (i.e., the SPM peak concentration without accompanying precipitation), the dust contribution on that day to the observed increased TDP can be small because the OS11 TDP sampler only opens its hatch during the precipitation as mentioned in Section 2.2. Note that we are also aware of the dust cloud transport above about 2 km during 18:00 UTC February 21 and 6:00 UTC February 22 (i.e., 3:00-15:00 JST February 22) in the lidar data (Fig. 7a,b; also see the NIES lidar-plot 090218-090222 website). However, the JMA observation at Toyama showed no precipitation during the time period (not shown). Therefore, we considered that this dust cloud above about 2 km also was not responsible for the observed increase of TDP during Event B in Fig. 2a. So our conclusion is that the increased SPM concentration with the very weak precipitation in the early morning on February 21 is the primary explanation for the relatively larger increase of the observed TDP for Event B in Fig. 2a.

As discussed by OS11, precipitation intensity may not be always responsible for the increased wet deposition amount (i.e., not necessary to have a proportional relationship). This suggests that in the real world, if the precipitation occurs “at the best (exact) timings of dust transport”, this kind of “very weak precipitation”, even during a short time period could possibly have power to significantly contribute to an increase in the wet deposition of dust. The relationship between weak precipitation and elevated pollution would be a good scientific topic in terms of deposition in future studies.

The current GEOS-5, however, could not significantly increase the TDP in the case of polluted dust in the atmosphere with such “very weak” precipitation as discussed below. As mentioned in Section 2.1, the GEOS-5 modelled wet deposition amount relies on scavenging efficiency, depending on updraft

velocity and convective cloud height (convective scavenging), and precipitation rate (large-scale scavenging) under the existence of the same amount of pollution. The other transport models also treated wet deposition process as a proportion of the precipitation amount (Mahowald et al., 1999; Zhao et al., 2003), which was also pointed out by OS11. Another global model treated the wet deposition as a proportion of the number concentration of raindrops for the sub-cloud scavenging (Takemura et al., 2000), which implies the relation to precipitation amount. Therefore, we can understand that modeled wet deposition amount is often proportional to the modelled precipitation, which is probably the standard treatment of chemical transport in the current global models as mentioned above. In this study, modelled weak precipitation in GEOS-5 also could not efficiently wash the atmospheric dust out as seen, for example, in a bubble plot from the EXP2 model run during the time period of OS11 (October 2008 – January 2010) (Fig. 9). Under the condition of low atmospheric column mass density of dust, wet deposition fluxes were less affected by precipitation amounts. On the other hand, even if the higher dust loading were seen, the wet deposition fluxes did not increase much under the “very weak” precipitation condition (i.e., closer to the x-axis). This suggests that the current parameterization of GEOS-5 model needs at least some precipitation amount even under the polluted condition, to significantly increase wet deposition amount. This could explain the still-existing large differences on TDP for Events B and C between the observations and GEOS-5 experiments to some extent in terms of the modelled wet scavenging efficiency.

3.4. Summary of the TDP performance at six Japanese locations within all the GEOS-5 experiments in January – April in 2009

Although the main focus of this study is TDP at Toyama, we additionally summarize the performance of the temporally re-sampled modeled TDP at all six of the OS11 measurement locations in Japan during the time period (January – April, 2009). The Root Mean Square Errors (RMSE) between the temporally re-sampled modeled TDP in each GEOS-5 experiment (EXP1-4) and the TDP observations at each location were calculated. Except for Nagoya and Hedo, overall, the assimilation of the aerosol data with the corrected MERRA precipitation (EXP4) showed the best performance, having the lowest values of RMSEs (Table 3). Although it is obvious that Event C at Toyama showed the largest observed TDP of the six locations during January – April 2009 (Fig. 2 of OS11; Fig. S2), it is also the case that the largest systematic improvement of the RMSEs as simulation complexity increased except for the case using the corrected MERRA precipitation in EXP3 (i.e., resolution and aerosol data assimilation) was also seen at Toyama within all the locations. This is probably due to the significant contributions from the large changes in the amount of the modeled TDP to the RMSEs on the big Asian dust event (Event C) from EXP1, EXP2, or EXP3 to EXP4 (Fig. 2). The other locations showed smaller RMSE differences than those at Toyama (Table 3). This confirms that our detailed comparisons at Toyama focusing on the TDP events in this study, thus far, could provide the most valuable and unique insights into the factors driving the TDP sensitivities associated with wet deposition process.

It is worth noting that the use of the corrected MERRA precipitation (EXP3) did not improve the simulated TDP relative to EXP2 (Table 3), actually performing worse at Sapporo, Toyama, Nagoya, and Tottori. The improvements in the RMSE at Fukuoka and Hedo were also very small. The TDP in EXP3 was reduced over the west coast of Japan, compared to EXP2 (see the blue-coloured grid cells over Japan

in Fig. S7c). This implies less dust available in EXP3 for deposition upon reaching Japan, compared to EXP2 (Fig. S7).

4. Conclusions and summary

During the January – April in 2009, OS11 observed two notable enhanced TDP events in Toyama, Japan: one in February (Event B) and another in March (Event C). As OS11 reported, the March 2009 event, Event C, was the largest TDP event observed among six Japanese observing sites during the time period of OS11 observations (Fig. 2 of OS11; Figs. 2a and S2). We focused and analysed the two observed TDP events at Toyama to examine model sensitivities on TDP at Toyama in different GEOS-5 settings and understand the reason why the OS11-observed TDP could largely increase. We used the results of four experiments with the NASA GEOS-5 model that included aerosols and were driven by the MERRA meteorology (see more about MERRA in Rienecker et al., 2011). The simulations systematically explored a hierarchy of complexities: (1) EXP1 was run at a coarse horizontal spatial resolution ($2^\circ \times 2.5^\circ$ latitude-by-longitude) (the outputs were obtained from YS14); (2) EXP2 was similar to EXP1 but was performed at $0.5^\circ \times 0.625^\circ$ horizontal spatial resolution (the outputs were obtained from YS14); (3) EXP3 was the same as EXP2 but additionally included the further constraint that the model generated precipitation was replaced by the corrected MERRA precipitation (see Section 2.1); (4) EXP4 was like EXP3 but additionally added a constraint on aerosol loading through data assimilation of AOD derived from the MODIS satellite instruments (the outputs were obtained from the so-called “MERRAero” aerosol reanalysis; see Section 2.1). This group of experiments could tell us the nature of dust transport and deposition over Toyama during the observed two TDP events, and the significance of model

configuration in reproducing the observations. The outcomes from this study will be useful for future field campaigns and support further research on topics related to dust deposition with GEOS-5.

Our findings from analysing the two TDP events at Toyama with some additional discussions are the following:

The higher spatial resolution simulations (EXP2-4) generally performed better than the coarser spatial resolution simulation (EXP1) in terms of the modeled TDP for Event C. One possible aspect of this is that considerably greater dust emissions were simulated over the source regions at higher resolution. One possible explanation for this is that the higher wind speeds over the source regions in EXP2 are the result of topographically driven flow being better resolved in that simulation, which is consistent with Nowotnick et al. (2011b), though we could not completely exclude other possible factors in this study. However, in any case, the seasonal mean column mass density of dust over Japan did not show much difference between EXP2 and EXP1 even if there were differences on the dust emissions around the dust source regions. Hence, we conclude that the dust emission differences did not matter and were not the primary reason for the increased TDP at Toyama for Event C. On the other hand, precipitation increased in EXP2 versus EXP1 at Toyama, and there was more TDP there. The increased spatial resolution apparently plays a role in increased simulated precipitation at Toyama. Again we speculate a direct role here for spatial resolution and topography: as Toyama is located near a mountain range it makes sense that orographic flow would play some role in determining local precipitation. Chao (2012) suggest a problem in that higher spatial resolution models generate excessive precipitation in the vicinity of steep topographic gradients. Indeed, the simulated precipitation in EXP2 exceeded the observed precipitation at Toyama. However, we emphasize that we cannot exclude other factors to contribute to the increased

precipitation at Toyama in this study. This argues for more work in the future to resolve issues of spatial resolution and the interplay with topography in both the source and sink processes involved in dust cycle modelling.

The use of aerosol data assimilation coupled with the corrected MERRA precipitation in EXP4 greatly increased the atmospheric dust burden over Toyama, and resulted in the best representation of the dust transport and TDP of the model experiments for Event C (Figs. 2 and 7). It is noteworthy that the impacts of (a) increasing horizontal resolution and (b) using the aerosol data assimilation on the modeled TDP were both large for Event C (Fig. 2a).

By contrast, use of the corrected MERRA precipitation alone (EXP3) did not obviously improve the simulated TDP compared to EXP2. These results suggest a role particularly for aerosol data assimilation (here, the MODIS AOD, but probably more generally) in significantly correcting model biases in terms of the simulated aerosol loading. However, the modeled TDP in EXP4 had yet still underestimated the observed TDP for Event C. The data assimilation experiment (EXP4) had significantly increased dust amount in the atmosphere, for which the value was the closest to the observation-based estimated TSP. In addition, the modeled precipitation was higher than what was observed (i.e. plenty of available precipitation for the wet removal in the model). This suggests that the parameterization of wet removal in GEOS-5 may be inadequate, which aerosol removal per unit of precipitation being probably underestimated. This approach—scaling wet removal to either precipitation rate or, equivalently, droplet number concentration (in the case of large scale precipitation), or to convective updraft mass fluxes (in the case of convective scale precipitation)—is typical of global aerosol models (e.g., Mahowald et al., 1999; Takemura et al., 2000; Zhao et al., 2003), and is generally ignoring microphysical relationships between

hydrometeor and aerosol size distributions and so inadequately representing scavenging efficiencies. Our results suggest this is an important area for further research.

While use of aerosol data assimilation resulted in the best simulation of TDP overall (EXP4), this improvement was especially apparent for Event C. By contrast, in Event B the aerosol data assimilation experiment was essentially the same as the other high resolution simulations (EXP2 and EXP3), all of which represented the observed TDP better than that coarse resolution experiment (EXP1). The increase of SPM in Toyama during Event B on February 21 was observed to correlate with very weak and short duration precipitation (Fig. 8). Our conclusion is that the observed TDP enhancement during Event B was probably driven by a fortuitous correlation of the increased surface level dust and the very weak short-time precipitation. This suggests that a real world linkage between even very weak and short duration precipitation with dust loading can be crucial to determining TDP. The results from the GEOS-5 experiments for Event B showed no systematic improvement in the modeled TDP across the higher resolution model experiments. Furthermore, the temporally re-sampled model mean precipitation rate in EXP2-4 during Event B exceeded what was observed (Fig. 2c), while the modeled TDP was much lower compared to the observed TDP. The aerosol data assimilation also did not help in this case; possibly because of cloudiness nearby or upwind location of Toyama (i.e., no available MODIS AOD data for the assimilation), or horizontal or vertical misplacement of the aerosol plume in the model. This suggests that the availability of the aerosol assimilation in time and space would significantly affect the errors of modeled TDP.

The results of our study should be useful for reducing biases in simulating the aerosol wet deposition process in future models. We emphasize three key aspects of the modelling which require further

consideration: (1) simulation of the dust loading magnitude at appropriate altitudes; (2) simulation of the timing (and magnitude) of precipitation in relation to timing of dust loading; and (3) the realism of the wet removal parameterization itself. Improved representation of these areas will be crucial to, for example, improving the simulation of deposition to snow and ice surfaces in the cryosphere, in order to reduce uncertainties on post-depositional processes such as the snow darkening effect (e.g., Warren and Wiscombe, 1980; Flanner et al., 2007, 2009; Painter et al., 2007; Aoki et al., 2006, 2011; Yasunari et al., 2011, 2014 (YS14), 2015; Niwano et al., 2012; Qian et al., 2015). In addition, better representation of aerosol deposition (especially dust) will help to reduce the uncertainties associated with changes in biological activity in the ocean related to iron fertilizations caused by dust depositions (Jickells et al., 2005, and references therein). Finally, a recent study by Yumimoto and Takemura (2015) showed a significant positive correlation between the satellite-derived chlorophyll data and their modeled dust deposition over the eastern North Pacific region, suggesting a possible relationship between Asian dust deposition and phytoplankton blooms there. The uncertainties related to these topics could possibly be reduced with the improvement of modelled wet deposition process of dust, based on the accumulation of many studies like this study. We hope these kinds of case studies with global models are further encouraged and valued in the scientific community.

Acknowledgements

The Science Mission Directorate at NASA Headquarters supported this study by the Aqua Terra Science Program and the Modeling, Analysis, and Prediction (MAP) Program. The GEOS-5 model development and the MERRAero project in the Global Modeling and Assimilation Office were also funded by NASA's MAP program. The GEOS-5 simulations were carried out in the system for NASA Center for Climate Simulation (NCCS). Max Suarez (NASA), Larry Takacs (SSAI), and Randy Koster (NASA), at NASA Goddard Space Flight Center (NASA/GSFC) kindly helped coding in GEOS-5, giving us useful information to understand GEOS-5 more, and had useful discussions on the model. Ravi Govindaraju (SSAI) helped the treatment of the outputs from the EXP4 GEOS-5 experiment (MERRAero). Useful comments and suggestions were provided by Anton Darmenov (NASA), Qian Tan (GESTAR/USRA), and Tetsuzo Yasunari (Research Institute for Humanity and Nature: RIHN) respectively. The lidar data at TESC maintained by NIES were used with helpful information provided by Atsushi Shimizu and Nobuo Sugimoto (NIES). The SPM data in Toyama were provided by TESC in Toyama prefecture. The authors gratefully acknowledge the NOAA Air Resources Laboratory (ARL) for the provision of the HYSPLIT transport and dispersion model and/or READY website (<http://ready.arl.noaa.gov>) used in this publication. Google Earth was used for distance calculation. Jan Angevine (ARTS) at NASA/GSFC proofread this paper.

References

- Adler, R. F., Huffman, G. J., Chang, A., Ferraro, R., Xie, P.-P., Janowiak, J., Rudolf, B., Schneider, U., Curtis, S., Bolvin, D., Gruber, A., Susskind, J., Arkin, P., Nelkin, E., 2003. The Version 2 Global Precipitation Climatology Project (GPCP) Monthly Precipitation Analysis (1979-Present). *J. Hydrometeor.*, 4, 1147-1167.
- Aoki, T., Motoyoshi, H., Kodama, Y., Yasunari, T. J., Sugiura, K., Kobayashi H., 2006. Atmospheric aerosol deposition on snow surfaces and its effect on albedo. *SOLA*, 2, 013-016, doi:10.2151/sola.2006-004.
- Aoki, T., Kuchiki, K., Niwano, M., Kodama, Y., Hosaka, M., Tanaka, T., 2011. Physically based snow albedo model for calculating broadband albedos and the solar heating profile in snowpack for general circulation models. *J. Geophys. Res.*, 116, D11114. doi:10.1029/2010JD015507.
- Bian, H., Colarco, P. P., Chin, M., Chen, G., Rodriguez, J. M., Liang, Q., Blake, D., Chu, D. A., da Silva, A., Darmenov, A. S., Diskin, G., Fuelberg, H. E., Huey, G., Kondo, Y., Nielsen, J. E., Pan, X., Wisthaler, A., 2013. Source attributions of pollution to the Western Arctic during the NASA ARCTAS field campaign. *Atmos. Chem. Phys.*, 13, 4707-4721, doi:10.5194/acp-13-4707-2013.
- Buchard, V., da Silva, A. M., Colarco, P., Krotkov, N., Dickerson, R. R., Stehr, J. W., Mount, G., Spinei, E., Arkinson, H. L., He, H., 2014. Evaluation of GEOS-5 sulfur dioxide simulations during the Frostburg, MD 2010 field campaign. *Atmos. Chem. Phys.*, 14, 1929–1941, doi:10.5194/acp-14-1929-2014.
- Buchard, V., da Silva, A. M., Colarco, P. R., Darmenov, A., Randles, C. A., Govindaraju, R., Torres, O., Campbell, J., Spurr, R., 2015. Using the OMI aerosol index and absorption aerosol optical depth to evaluate the NASA MERRA Aerosol Reanalysis. *Atmos. Chem. Phys.*, 15, 5743-5760,

doi:10.5194/acp-15-5743-2015.

- Chao, W. C. (2012). Correction of Excessive Precipitation over Steep and High Mountains in a GCM. *J. Atmos. Sci.*, 69(5), 1547–1561, doi:10.1175/JAS-D-11-0216.1.
- Chao, W. C. (2015). Correction of excessive precipitation over steep and high mountains in a GCM: A simple method of parameterizing the thermal effects of subgrid topographic variation. *J. Atmos. Sci.*, 72, 2366-2378, doi:10.1175/JAS-D-14-0336.1.
- Chin, M., Rood, R. B., Lin, S.-J., Muller, J. F., Thompson, A. M., 2000. Atmospheric sulfur cycle in the global model GOCART: Model description and global properties. *J. Geophys. Res.*, 105(D20), 24671-24687, doi:10.1029/2000JD900384.
- Chin, M., Ginoux, P., Kinne, S., Holben, B. N., Duncan, B. N., Martin, R. V., Logan, J. A., Higurashi, A., Nakajima, T., 2002. Tropospheric aerosol optical thickness from the GOCART model and comparisons with satellite and sunphotometer measurements. *J. Atmos. Sci.*, 59, 461-483.
- Colarco P., da Silva, A., Chin, M., Diehl, T., 2010. Online simulations of global aerosol distributions in the NASA GEOS-4 model and comparisons to satellite and ground-based aerosol optical depth. *J. Geophys. Res.*, 115, D14207, doi:10.1029/2009JD012820.
- Colarco, P. R., Nowottnick, E. P., Randles, C. A., Yi, B., Yang, P., Kim, K.-M., Smith, J. A., Bardeen, C. G., 2014a. Impact of radiatively interactive dust aerosols in the NASA GEOS-5 climate model: Sensitivity to dust particle shape and refractive index. *J. Geophys. Res. Atmos.*, 119, 753–786, doi:10.1002/2013JD020046.
- Colarco, P. R., Kahn, R. A., Remer, L. A., Levy, R. C., 2014b. Impact of satellite viewing-swath width on global and regional aerosol optical thickness statistics and trends. *Atmos. Meas. Tech.*, 7, 2313–2335,

doi:10.5194/amt-7-2313-2014.

Darmenova, K., Sokolik, I. N., Darmenov, A., 2005. Characterization of east Asian dust outbreaks in the spring of 2001 using ground-based and satellite data. *J. Geophys. Res.*, 110, D02204, doi:10.1029/2004JD004842.

Draxler, R. R., Rolph, G. D., 2014. HYSPLIT (HYbrid Single-Particle Lagrangian Integrated Trajectory) Model access via NOAA ARL READY Website (<http://ready.arl.noaa.gov/HYSPLIT.php>). NOAA Air Resources Laboratory, Silver Spring, MD.

Duce, R. A., Unni, C. K., Ray, B. J., Prospero, J. M., Merrill, J. T., 1980. Long-range atmospheric transport of soil dust from Asia to the tropical North Pacific: Temporal and variability. *Science*, 209(4464), 1,522-1,524, doi:10.1126/science.209.4464.1522.

Emori, S., Nozawa, T., Abe-Ouchi, A., Numaguti, A., Kimoto, M., Nakajima, T., 1999. Coupled ocean-atmosphere model experiments of future climate change with an explicit representation of sulfate aerosol scattering. *J. Meteor. Soc. Jpn.*, 77, 1299-1307.

Flanner, M. G., Zender, C. S., Randerson, J. T., Rasch, P. J., 2007. Present-day climate forcing and response from black carbon in snow. *J. Geophys. Res.*, 112, D11202, doi:10.1029/2006JD008003.

Flanner, M. G., Zender, C. S., Hess, P. G., Mahowald, N. M., Painter, T. H., Ramanathan, V., Rasch, P. J., 2009. Springtime warming and reduced snow cover from carbonaceous particles. *Atmos. Chem. Phys.*, 9(7), 2481-2497, doi:10.5194/acp-9-2481-2009.

Ginoux, P., Chin, M., Tegen, I., Prospero, J. M., Holben, B., Dubovik, O., Lin, S.-J., 2001. Sources and distributions of dust aerosols simulated with the GOCART model. *J. Geophys. Res.*, 106(D17), 20255-20273, doi:10.1029/2000JD000053.

- Hao, Q., Matsumoto, M., Mizoguchi T., 1995. Studies on estimation of Kosa event from analysis of suspended particulate matter (SPM) by β -ray absorption method. *Eurozoru Kenkyu*, 10, 41-50 (in Japanese with English abstract).
- Hara, Y., Yumimoto K., Uno, I., Shimizu, A., Sugimoto, N., Liu, Z., Winker, D. M., 2009. Asian dust outflow in the PBL and free atmosphere retrieved by NASA CALIPSO and an assimilated dust transport model. *Atmos. Chem. Phys.*, 9, 1227–1239, doi:10.5194/acp-9-1227-2009.
- Hansen, J., Sato, M., Ruedy, R., Kharecha, P., Lacis, A., Miller, R., Nazarenko, L., Lo, K., Schmidt, G. A., Russell, G., Aleinov, I., Bauer, S., Baum, E., Cairns, B., Canuto, V., Chandler, M., Cheng, Y., Cohen, A., Del Genio, A., Faluvegi, G., Fleming, E., Friend, A., Hall, T., Jackman, C., Jonas, J., Kelley, M., Kiang, N. Y., Koch, D., Labow, G., Lerner, J., Menon, S., Novakov, T., Oinas, V., Perlwitz, Ja., Perlwitz, Ju., Rind, D., Romanou, A., Schmunk, R., Shindell, D., Stone, P., Sun, S., Streets, D., Tausnev, N., Thresher, D., Unger, N., Yao, M., Zhang, S., 2007. Dangerous human-made interference with climate: a GISS modelE study. *Atmos. Chem. Phys.*, 7, 2287-2312, doi:10.5194/acp-7-2287-2007.
- Hill, C., DeLuca, C., Suarez, M., da Silva, A., 2004. The architecture of the earth system modeling framework, *Comput. Sci. Eng.*, 6(1), 18-28, doi: 10.1109/MCISE.2004.1255817.
- Inomata, Y., Igarashi, Y., Mikami, M., Tanaka, T. Y., Chiba, M., 2009. Seasonal and yearly variations of dust deposition in Tsukuba: Possible linkage with variations of dust emission over the Asian continent. *SOLA*, 5, 153-156, doi:10.2151/sola.2009-039.
- Iwasaka, Y., Minoura, H., Nagaya, K., 1983. The transport and special scale of Asia dust-storm cloud: a case study of the dust-storm event of April 1979. *Tellus B*, 35B, 189-196,

doi:10.1111/j.1600-0889.1983.tb00023.x.

Iwasaka, Y. 1986a. Measurement of depolarization of stratospheric particles by lidar—A case study on the disturbed stratospheric aerosol layer by the volcanic eruption of Mt. El Chichon. *J. Geomag. Geoelectr.* 38, 729–740.

Iwasaka, Y. 1986b. Non-spherical particles in the antarctic polar stratosphere—increase in particulate content and stratospheric water vapor budget. *Tellus B*, 38B, 364–374, doi:10.1111/j.1600-0889.1986.tb00261.x.

Iwasaka, Y., Yamato, M., Imasu, R., Ono, A., 1988. Transport of Asian dust (KOSA) particles; importance of weak KOSA events on the geochemical cycle of soil particles. *Tellus B*, 40B, 494–503, doi:10.1111/j.1600-0889.1988.tb00119.x.

Jickells, T. D., An, Z. S., Andersen, K. K., Baker, A. R., Bergametti, G., Brooks, N., Cao, J. J., Boyd, P. W., Duce, R. A., Hunter, K. A., Kawahata, H., Kubilay, N., laRoche, J., Liss, P. S., Mahowald, N., Prospero, J. M., Ridgwell, A. J., Tegen, I., Torres, R., 2005. Global iron connections between desert dust, ocean biogeochemistry, and climate. *Science*, 308(5718), 67–71, doi: 10.1126/science.1105959.

Kasahara, M., 2002. The present state and future assignments of air pollution by particulate matter—The meaning of innovation of PM_{2.5} — . *J. Jpn. Soc. Atmos. Environ.*, 37(2), 96–107, doi:10.11298/taiki1995.37.96 (in Japanese with English abstract).

Kessner, A. L., Wang J., Levy, R. C., Colarco, P. R., 2013. Remote sensing of surface visibility from space: A look at the United States East Coast. *Atmos. Environ.*, 81, 136–147, doi:10.1016/j.atmosenv.2013.08.050.

Kido, M., Nakamura T., Yamazaki, T., Mizoguchi, T., Kondo, T., Toriyama S., Hashimoto, J., Kawasaki,

- K., 2007. Study on atmospheric deposition in East Asia (the first report)— Concentration of chemical constituents in atmospheric aerosol particles during Kosa events in Toyama —. Annual Report of Toyama Prefectural Environmental Science Research Center, 35, 69-75 (in Japanese).
- Lawrence, M. G., Rasch, P. J., von Kuhlmann, R., Williams, J., Fischer, H., de Reus, M., Lelieveld, J., Crutzen, P. J., Schultz, M., Stier, P., Huntrieser, H., Heland, J., Stohl, A., Forster, C., Elbern, H., Jakobs, H., Dickerson, R. R., 2003. Global chemical weather forecasts for field campaign planning: predictions and observations of large-scale features during MINOS, CONTRACE, and INDOEX. *Atmos. Chem. Phys.*, 3, 267-289, doi:10.5194/acp-3-267-2003.
- Liu, H., Jacob, D. J., Bey, I., Yantosca, R. M., 2001. Constraints from ^{210}Pb and ^7Be on wet deposition and transport in a global three-dimensional chemical tracer model driven by assimilated meteorological fields. *J. Geophys. Res.*, 106(D11), 12109-12128, doi:10.1029/2000JD900839.
- Luo, C., Mahowald, N. M., del Corral, J., 2003. Sensitivity study of meteorological parameters on mineral aerosol mobilization, transport, and distribution. *J. Geophys. Res.*, 108(D15), 4447, doi:10.1029/2003JD003483.
- Mahowald, N., Kohfeld, K., Hansson, M., Balkanski, Y., Harrison, S. P., Prentice, I. C., Schulz, M., Rodhe, H., 1999. Dust sources and deposition during the last glacial maximum and current climate: A comparison of model results with paleodata from ice cores and marine sediments. *J. Geophys. Res.*, 104(D13), 15895–15916, doi:10.1029/1999JD900084.
- Mahowald, N. M., Baker, A. R., Bergametti, G., Brooks, N., Duce, R. A., Jickells, T. D., Kubilay, N., Prospero, J. M., Tegen, I., 2005. Atmospheric global dust cycle and iron inputs to the ocean. *Global Biogeochem. Cy.*, 19(4), GB4025, doi:10.1029/2004GB002402.

- Mahowald, N. M., Engelstaedter, S., Luo, C., Sealy, A., Artaxo, P., Benitez-Nelson, C., Bonnet, S., Chen, Y., Chuang, P. Y., Cohen, D. D., Dulac, F., Herut, B., Johansen, A. M., Kubilay, N., Losno, R., Maenhaut, W., Paytan, A., Prospero, J. M., Shank, L. M., Siefert, R. L., 2009. Atmospheric iron deposition: Global distribution, variability, and human perturbations. *Annu. Rev. Mar. Sci.*, 1, 245–278, doi:10.1146/annurev.marine.010908.163727.
- Matoba, S., Mori, I., Hayakari, S., Nishikawa, M., 2005. New method of detecting Kosa (Asian dust) from SPM data measured by environmental air monitoring stations. *J. Aerosol Res. (Eaorozoru Kenkyu)*, 20(3), 225-230, doi:10.11203/jar.20.225 (in Japanese with English abstract).
- Molod, A., Takacs, L., Suarez, M., Bacmeister, J., Song, I.-S., and Eichmann, A., 2012. The GEOS-5 Atmospheric General Circulation Model: Mean Climate and Development from MERRA to Fortuna. Technical Report Series on Global Modeling and Data Assimilation, NASA/TM-2012-104606, 28 (available at: <http://gmao.gsfc.nasa.gov/pubs/tm/docs/Molod484.pdf>).
- Mizoguchi, T., Kawasaki, K., Shimizu, A., Satake, H., 2009. Investigation of dry deposition in Toyama and analysis by rider during the period of high SPM concentration. *J. Jpn. Soc. Atmos. Environ.*, 44(3), 155-165, doi:10.11298/taiki.44.155 (in Japanese with English abstract; note that “rider” for the original title above should be “lidar” but we put the title as it is for this reference).
- Niwano, M., Aoki, T., Kuchiki, K., Hosaka, M., Kodama, Y., 2012. Snow Metamorphism and Albedo Process (SMAP) model for climate studies: Model validation using meteorological and snow impurity data measured at Sapporo, Japan. *J. Geophys. Res.*, 117, F03008, doi:10.1029/2011JF002239.
- Nowotnick, E., Colarco, P., Ferrare, R., Chen, G., Ismail, S., Anderson, B., Browerll, E., 2010. Online

simulations of mineral dust aerosol distributions: Comparisons to NAMMA observations and sensitivity to dust emission parameterization. *J. Geophys. Res.*, 115, D03202, doi:10.1029/2009JD012692.

Nowottnick, E., Colarco P., da Silva, A., Hlavka, D., McGill, M., 2011a. The fate of saharan dust across the atlantic and implications for a central american dust barrier. *Atmos. Chem. Phys.*, 11, 8415–8431, doi:10.5194/acp-11-8415-2011.

Nowottnick, E. P., Colarco, P. R., da Silva, A., 2011b. Effects of spatial resolution on the simulated dust aerosol lifecycle: Implications for dust event magnitude and timing in the NASA GEOS-5 AGCM. Abstract A53C-0369 presented at 2011 Fall Meeting, AGU, San Francisco, Calif., 5-9 Dec.

Nowottnick, E. P., Colarco, P. R., Welton, E. J., da Silva, A., 2015. Use of the CALIOP vertical feature mask for evaluating global aerosol models. *Atmos. Meas. Tech. Discuss.*, 8, 1401-1455, doi:10.5194/amtd-8-1401-2015.

Osada, K., Iida, H., Kido, M., Matsunaga, K., Iwasaka, Y., 2004. Mineral dust layers in snow at Mount Tateyama, Central Japan: Formation processes and characteristics. *Tellus B*, 56, 382-392, doi: 10.1111/j.1600-0889.2004.00108.x.

Osada, K., Ura, S., Kagawa, M., Mikami, M., Tanaka, T. Y., Matoba, S., Aoki, K., Shinoda, M., Kurosaki, Y., Hayashi, M., Shimizu, A., Uematsu, M., 2011. Temporal and Spatial Variations of Wet Deposition Flux of Mineral Dust in Japan. *SOLA*, 7, 49-52, doi:10.2151/sola.2011-013.

Osada, K., Ura, S., Kagawa, M., Mikami, M., Tanaka, T. Y., Matoba, S., Aoki, K., Shinoda, M., Kurosaki, Y., Hayashi, M., Shimizu, A., Uematsu, M., 2014. Wet and dry deposition of mineral dust particles in Japan: factors related to temporal variation and spatial distribution. *Atmos. Chem. Phys.*, 14,

1107-1121, doi:10.5194/acp-14-1107-2014.

- Painter, T. H., Barrett, A. P., Landry, C. C., Neff, J. C., Cassidy, M. P., Lawrence, C. R., McBride, K. E., Farmer, G. L., 2007. Impact of disturbed desert soils on duration of mountain snow cover. *Geophys. Res. Lett.*, 34, L12502, doi: 10.1029/2007GL030284.
- Putman, W. M., Suarez, M., 2011. Cloud-system resolving simulations with the NASA Goddard Earth Observing System global atmospheric model (GEOS-5). *Geophys. Res. Lett.*, 38, L16809, doi:10.1029/2011GL048438.
- Qian, Y., Yasunari, T. J., Doherty, S. J., Flanner, M. G., Lau, W. K. M., Ming, J., Wang, H., Wang, M., Warren, S. G., Zhang, R., 2015. Light-absorbing particles in snow and ice: Measurement and modeling of climatic and hydrological impact, *Adv. Atmos. Sci.*, 32(1), 64-91, doi: 10.1007/s00376-014-0010-0.
- Randles, C. A., Colarco, P. R., da Silva, A., 2013. Direct and semi-direct aerosol effects in the NASA GEOS-5 AGCM: aerosol-climate interactions due to prognostic versus prescribed aerosols. *J. Geophys. Res. Atmos.*, 118, 149–169, doi:10.1029/2012JD018388.
- Reichle, R. H., Liu, Q., 2014. Observation-Corrected Precipitation Estimates in GEOS-5. Technical Report Series on Global Modeling and Data Assimilation, NASA/TM–2014-104606, 35 (available at: <http://gmao.gsfc.nasa.gov/pubs/docs/Reichle734.pdf>).
- Reynolds, R. W., Rayner, N. A., Smith, T. M., Stokes, D. C., Wang, W., 2002. An improved in situ and satellite SST analysis for climate. *J. Clim.*, 15, 1609-1625.
- Rienecker, M. M., Suarez, M. J., Todling, R., Bacmeister, J., Takacs, L., Liu, H.-C., Gu, W., Sienkiewicz, M., Koster, R. D., Gelaro, R., Stajner, I., Nielsen, J. E., 2008. The GEOS-5 Data Assimilation System

- Documentation of Versions 5.0.1, 5.1.0, and 5.2.0. Technical Report Series on Global Modeling and Data Assimilation, NASA/TM-2008-104606, 27 (available at: <http://gmao.gsfc.nasa.gov/pubs/docs/Rienecker369.pdf>).

Rienecker, M. M., Suarez, M. J., Gelaro, R., Todling, R., Bacmeister, J., Liu, E., Bosilovich, M. G., Schubert, S. D., Takacs, L., Kim, G.-K., Bloom, S., Chen, J., Collins, D., Conaty, A., da Silva, A., Gu, W., Joiner, J., Koster, R. D., Lucchesi, R., Molod, A., Owens, T., Pawson, S., Pegion, P., Redder, C., Reichle, R., Robertson, F. R., Ruddick, A. G., Sienkiewicz, M., Woollen, J., 2011. MERRA - NASA's Modern-Era Retrospective Analysis for Research and Applications. *J. Clim.*, 24, 3624-3648, doi:10.1175/JCLI-D-11-00015.1.

Rolph, G. D., 2014. Real-time Environmental Applications and Display sYstem (READY) Website (<http://ready.arl.noaa.gov>). NOAA Air Resources Laboratory, Silver Spring, MD.

Sanap, S. D., Ayantika, D. C., Pandithurai, G., Niranjana, K., 2014. Assessment of the aerosol distribution over Indian subcontinent in CMIP5 models. *Atmos. Environ.*, 87, 123-137, doi:10.1016/j.atmosenv.2014.01.017.

Shaw, G. E., 1980. Transport of Asian desert aerosol to the Hawaiian Islands. *J. Appl. Meteorol.*, 19, 1254- 1259.

Shimizu, A., Sugimoto, N., Matsui, I., Arao, K., Uno, I., Murayama, T., Kagawa, N., Aoki, K., Uchiyama, A., Yamazaki, A., 2004. Continuous observations of Asian dust and other aerosols by polarization lidars in China and Japan during ACE-Asia. *J. Geophys. Res.*, 109, D19S17, doi:10.1029/2002JD003253.

Sugimoto, N., Uno, I., Nishikawa, M., Shimizu, A., Matsui, I., Dong, X., Chen, Y., Quan, H., 2003.

Record heavy Asian dust in Beijing in 2002: Observations and model analysis of recent events. *Geophys. Res. Lett.*, 30(12), 1640, doi:10.1029/2002GL016349.

Sugimoto, N., Matsui, I., Shimizu, A., Nishizawa, T., Hara, Y., Xie, C., Uno, I., Yumimoto, K., Wang, Z., Yoon, S.-C., 2008. Lidar network observations of tropospheric aerosols. *Proc. SPIE 7153, Lidar Remote Sensing for Environmental Monitoring IX*, 71530A, doi: 10.1117/12.806540.

Takemura T., Okamoto, H., Maruyama, Y., Numaguti, A., Higurashi, A., Nakajima, T., 2000. Global three-dimensional simulation of aerosol optical thickness distribution of various origins. *J. Geophys. Res.*, 105(D14), 17853-17873, doi:10.1029/2000JD900265.

Takemura T., Nakajima, T., Dubovik, O., Holben, B. N., Kinne, S., 2002. Single-Scattering Albedo and Radiative Forcing of Various Aerosol Species with a Global Three-Dimensional Model. *J. Clim.*, 15, 333-352.

Taylor, K. E., Stouffer, R. J., Meehl, G. A., 2012. An Overview of CMIP5 and the Experiment Design. *Bull. Amer. Meteor. Soc.*, 93, 485–498, doi:10.1175/BAMS-D-11-00094.1.

Tegen, I., Lacis, A. A., 1996. Modeling of particle size distribution and its influence on the radiative properties of mineral dust aerosol. *J. Geophys. Res.*, 101(D14), 19237–19244, doi:10.1029/95JD03610.

Uematsu, M., Duce, R. A., Prospero, J. M., 1985. Deposition of atmospheric mineral particles in the North Pacific Ocean. *J. Atmos. Chem.*, 3, 123-138.

Uno, F., Kawase, H., Ishizaki, N. N., Yoshikane, T., Hara, M., Kimura, F., Iyobe, T., Kawashima, K., 2014. Analysis of regional difference in altitude dependence of snow depth using high resolve numerical experiments. *SOLA*, 10, 19–22, doi: 10.2151/sola.2014-005.

- Uno, I., Eguchi, K., Yumimoto, K., Takemura, T., Shimizu, A., Uematsu, M., Liu, Z., Wang, Z., Hara, Y., Sugimoto, N., 2009. Asian dust transported one full circuit around the globe. *Nat. Geosci.*, 2, 557-560, doi:10.1038/NGEO583.
- Ura, S., Osada, K., Kagawa, M., Mikami, M., Matoba, S., Aoki, K., Shinoda, M., Kusoraki, Y., Hayashi, M., Shimizu, A., Uematsu, M., 2011. Estimation of mineral dust amount using Fe content in water-insoluble residue of atmospheric deposition samples. *Eurozoru Kenkyu*, 26(3), 234-241, doi: 10.11203/jar.26.234 (in Japanese with English abstract).
- Warren, S. G., Wiscombe, W. J., 1980. A Model for the Spectral Albedo of Snow . II : Snow Containing Atmospheric Aerosols. *J. Atmos. Sci.*, 37, 2734-2745.
- Xie, P., Chen, M., Yang, S., Yatagai, A., Hayasaka, T., Fukushima, Y., Liu, C., 2007. A gauge-based analysis of daily precipitation over East Asia. *J. Hydrometeor*, 8, 607–626, doi: 10.1175/JHM583.1.
- Yasunari, T. J., Shiraiwa, T., Kanamori, S., Fujii, Y., Igarashi, M., Yamazaki, K., Benson, C. S., Hondoh, T., 2007. Intra-annual variations in atmospheric dust and tritium in the North Pacific region detected from an ice core from Mount Wrangell, Alaska. *J. Geophys. Res.*, 112, D10208, doi:10.1029/2006JD008121.
- Yasunari, T. J., Yamazaki, K., 2009a. Impacts of Asian dust storm associated with the stratosphere-to-troposphere transport in the spring of 2001 and 2002 on dust and tritium variations in Mount Wrangell ice core, Alaska. *Atmos. Environ.*, 43, 2582-2590, doi: 10.1016/j.atmosenv.2009.02.025.
- Yasunari, T. J., Yamazaki, K., 2009b. Origins of air masses over an Alaskan glacier and implications for ice core studies in the North Pacific region. *SOLA*, 5, 77-80, doi: 10.2151/sola.2009-020.

- Yasunari, T. J., Koster, R. D., Lau, K. M., Aoki, T., Sud, Y. C., Yamazaki, T., Motoyoshi, H., Kodama, Y., 2011. Influence of dust and black carbon on the snow albedo in the NASA Goddard Earth Observing System version 5 land surface model. *J. Geophys. Res.*, 116, D02210, doi:10.1029/2010JD014861.
- Yasunari, T. J., Lau, K.-M., Mahanama, S. P. P., Colarco, P. R., da Silva, A. M., Aoki, T., Aoki, K., Muraio, N., Yamagata, S., Kodama, Y., 2014. GODDARD SNOW IMPURITY MODULE (GOSWIM) FOR THE NASA GEOS-5 EARTH SYSTEM MODEL: PRELIMINARY COMPARISONS WITH OBSERVATIONS IN SAPPORO, JAPAN. *SOLA*, 10, 50-56, doi:10.2151/sola.2014-011.
- Yasunari, T. J., Koster, R. D., Lau, W. K. M., Kim, K.-M., 2015. Impact of snow darkening via dust, black carbon, and organic carbon on boreal spring climate in the Earth system, *J. Geophys. Res. Atmos.*, 120, 5485–5503, doi:10.1002/2014JD022977.
- Yu, H., Dickinson, R. E., Chin, M., Kaufman, Y. J., Holben, B. N., Geogdzhayev, I. V., Mishchenko, M. I., 2003. Annual cycle of global distributions of aerosol optical depth from integration of MODIS retrievals and GOCART model simulations. *J. Geophys. Res.*, 108, 4128, doi:10.1029/2002JD002717.
- Yu, H., Remer, L. A., Chin, M., Bian, H., Tan, Q., Yuan, T., Zhang, Y., 2012. Aerosol from overseas rival domestic emissions over North America. *Science*, 337(6094), 566-569, doi:10.1126/science.1217576.
- Yumimoto, K., Eguchi, K., Uno, I., Takemura, T., Liu, Z., Shimizu, A., Sugimoto, N., Strawbridge, K., 2010. Summertime trans-Pacific transport of Asian dust. *Geophys. Res. Lett.*, 37, L18815, doi:10.1029/2010GL043995.
- Yumimoto, K., Takemura T., 2015. Long-term Inverse Modeling of Asian Dust: Inter-annual Variations of

Yasunari et al. (2015), Atmospheric Research.

Its Emission, Transport, Deposition and Radiative Forcing. *J. Geophys. Res. Atmos.*, doi: 10.1002/2014JD022390, in press.

Zhao, T. L., Gong, S. L., Zhang, X. Y., McKendry, I. G., 2003. Modeled size-segregated wet and dry deposition budgets of soil dust aerosol during ACE-Asia 2001: Implications for trans-Pacific transport, *J. Geophys. Res.* 108, 8665, doi:10.1029/2002JD003363, D23.

ACCEPTED MANUSCRIPT

Figure captions

Fig. 1. Surface geopotential height in (a) EXP1 (144x91) and (b) EXP2 (576x361) GEOS-5 simulations with 6 locations (circles) for the observed TDP by OS11. For EXP1, the Toyama and Nagoya locations are located in the same grid point.

Fig. 2. Comparisons of TDP, atmospheric aerosol, and precipitation data to GEOS-5 data (EXP1-4) at Toyama during January – April in 2009. (a) The observed (in blue; including Events B and C with the labels) and the temporally re-sampled GEOS-5 modeled TDP data (plots shown in red, light blue, yellowish green, and purple correspond to EXP1, 2, 3, and 4, respectively; the same colors applied to the modeled data in the other panels). (b) Comparisons between the temporally re-sampled mean observed SPM concentration in Toyama city (in blue; 9-location average) and the temporally re-sampled mean GEOS-5 surface mass concentrations of dust (EXP1-4). Estimated TSP concentration computed from the re-sampled mean SPM data with Eq. 2 in Fig. S3a is also shown in gray. (c) Comparisons between the temporally re-sampled JMA-observed and GEOS-5 daily precipitation rates (EXP1-4). In the data of OS11, there are slight time lags between sampling times but we continuously plotted. When each sampling time period was not fully within the time period during January 2009 to April 2009, the data were not used for plotting.

Fig. 3. Accumulated dust emission fluxes during January – April in 2009 from the GEOS-5 experiments (grid-filled in rainbow colors) in two different horizontal resolutions (a: EXP1; b: EXP2) with mean 10-m wind velocity (white contours in m s^{-1}). (c) The differences between the two experiments (EXP2 minus

EXP1) of the dust emission fluxes (grid-filled from blue to red) and mean 10-m wind velocity (green contour). For the difference, the data from EXP2 were re-gridded into the same horizontal resolution of EXP1.

Fig. 4. Similar to Fig. 3 but for mean column mass density of dust in January – April in 2009 from the two GEOS-5 experiments (a: EXP1; b: EXP2; grid-filled in rainbow colors; seasonally averaged from daily mean outputs). (c) The difference between the two experiments (EXP2 minus EXP1; grid-filled from blue to red). For the difference, the data from EXP2 were re-gridded into the same horizontal resolution of EXP1.

Fig. 5. Similar to Fig. 3 but for accumulated modeled TDP from the two GEOS-5 experiments during January – April in 2009 (a: EXP1; b: EXP2; grid-filled in rainbow colors) with the observed OS11 TDP at six locations (circles filled with the same scale in rainbow) for the same time period as shown in Table 1 of OS11. (c) The difference between the two experiments (EXP2 minus EXP1; grid-filled from blue to red), the data from EXP2 were re-gridded into the same horizontal resolution of EXP1.

Fig. 6. Longitude-pressure cross section at the closest latitude of the OS11 Toyama site on March 16, 2009, in EXP1 (top panel) and EXP2 (bottom panel) on specific humidity (kg kg^{-1} ; contours shaded in colors), dust mass concentration (mg m^{-3} ; only plotted if the concentration was $\geq 0.05 \text{ mg m}^{-3}$; white contours), and vertical velocity (ω ; Pa s^{-1} ; only plotted if the values $\leq 0 \text{ Pa s}^{-1}$, i.e., upward motion; black contours; dashed lines showed negative values). The OS11 Toyama site is at 36.70°N and 137.19°E , and the closest

grid points to the site are 36.0°N and 137.5°E in EXP1, and 36.5°N and 137.5°E in EXP2, respectively.

Fig. 7. Comparisons of simulated dust transport to Toyama in the winter-spring of 2009. All data are in UTC. The lidar data at TESC is shown (a: attenuated backscatter coefficient, ABC, at 532 nm; b: depolarization ratio, DR, at 532 nm). For the GEOS-5 data at the closest grid points to the OS11 Toyama site (c: EXP4; d: EXP2; e: EXP1), the shaded contours and solid line with point (right side scale) denote vertical profile of daily mean mass concentrations of dust (mg m^{-3}) and daily precipitation rate (mm day^{-1}), respectively. The vertical pressure levels from 900 to 300 hPa are shown in log scale. See the information of the lidar data and OS11 sites in Section 2.2.

Fig. 8. Comparisons between 1-hourly observed SPM concentration provided by TESC (nine-location average in Toyama city) and JMA-observed 1-hourly precipitation rate at the JMA Toyama station obtained from the JMA website (see the main text) during February 18-25, 2009. The 1-hourly JMA precipitation data on February 20 and 21 were only picked up and used for the precipitation plots corresponding to the first and second high SPM days (blue and red bars, respectively). The missing SPM data at a certain location was removed from the nine-location average.

Fig. 9. The relationships at Toyama in the GEOS-5 modeled data from EXP2 among daily mean column mass density of dust, daily precipitation rate, and daily wet deposition flux of dust during the defined precipitation events (see Section 2.1). The time period covers October 2008 to January 2010, which is the time period of OS11 as shown in their Fig. 2 (also in Fig. S2). The bubble sizes, which correspond to the

amounts of wet deposition flux of dust, were automatically scaled in the plotting software (grapher 9; Golden Software, Inc.), using the minimum and maximum values within the available data.

ACCEPTED MANUSCRIPT

Figure 1

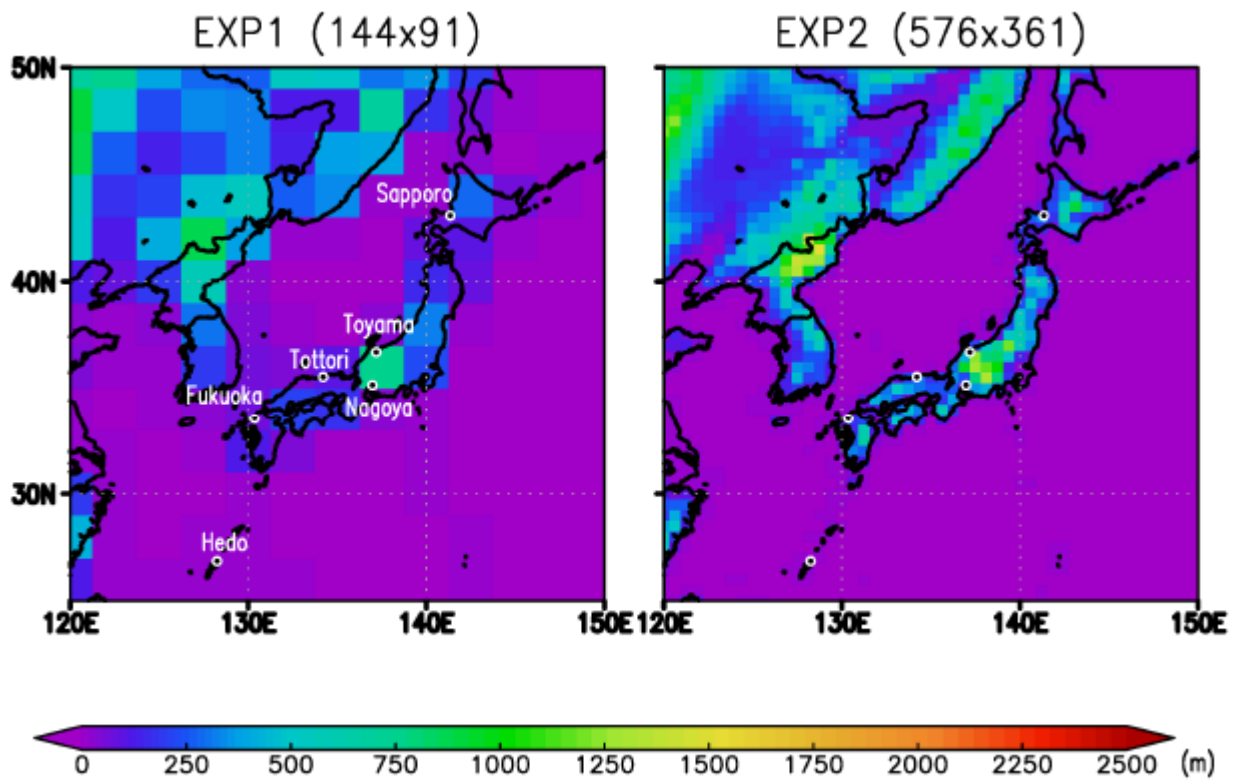


Figure 2

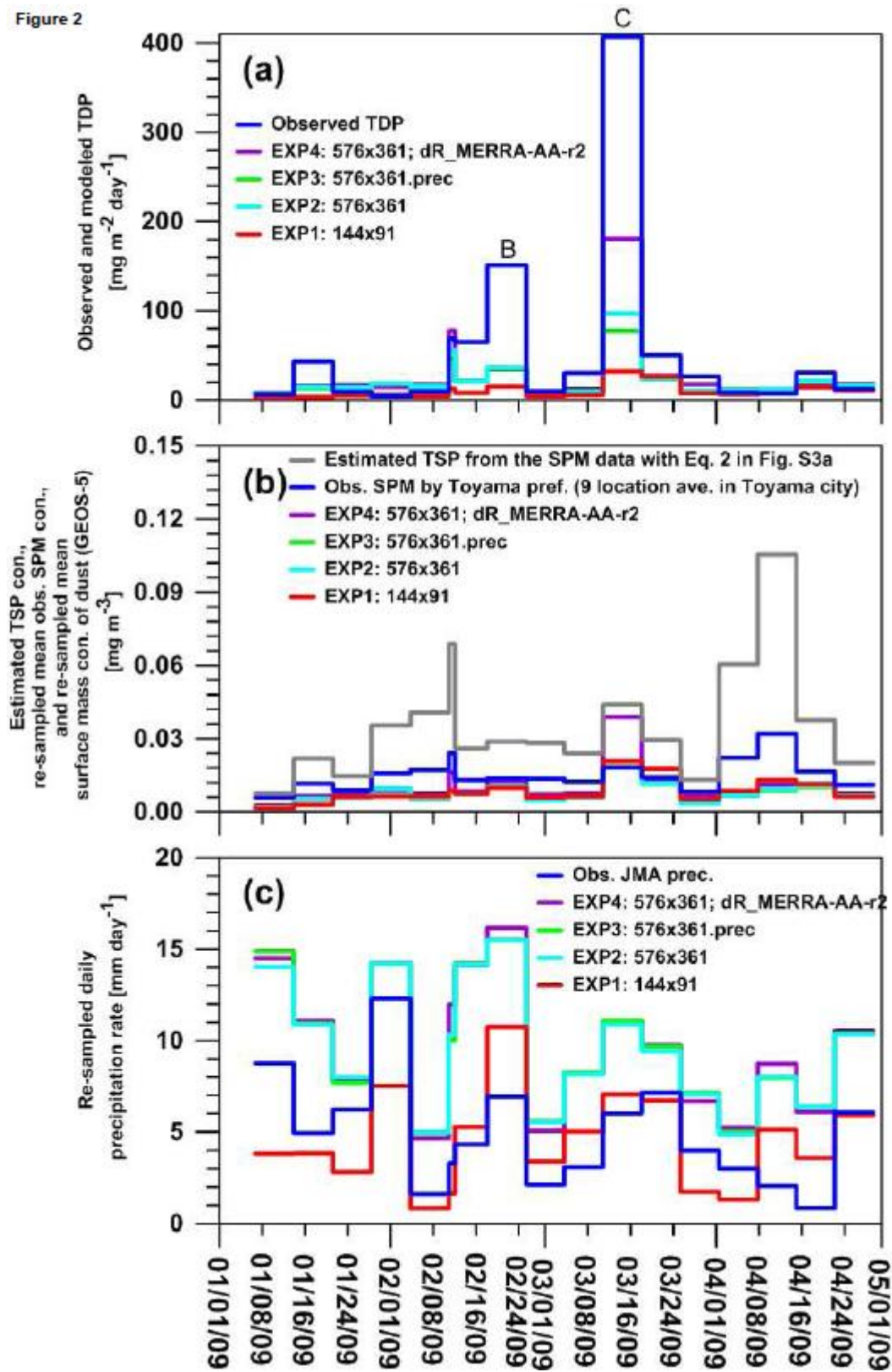


Figure 3

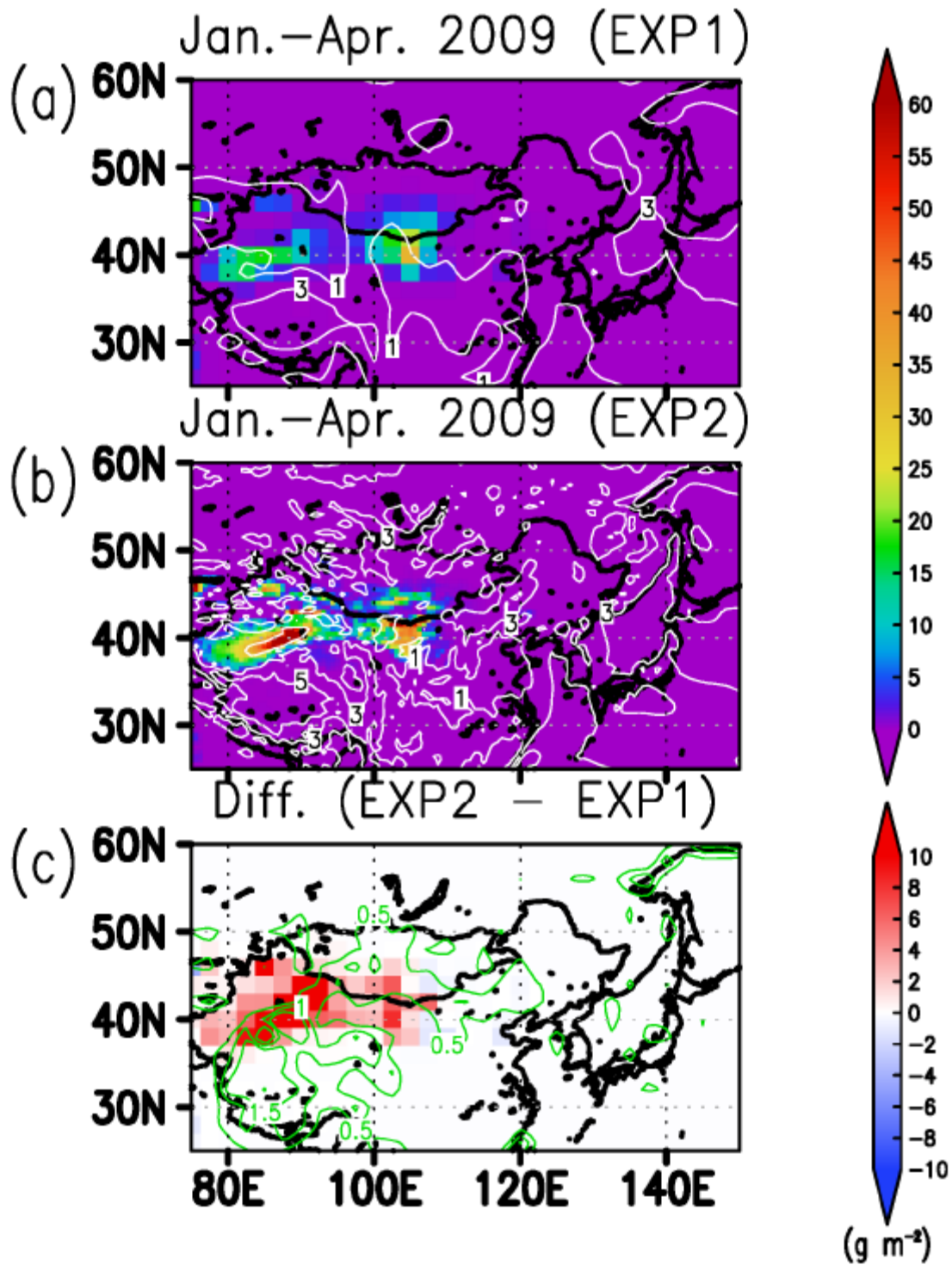


Figure 4

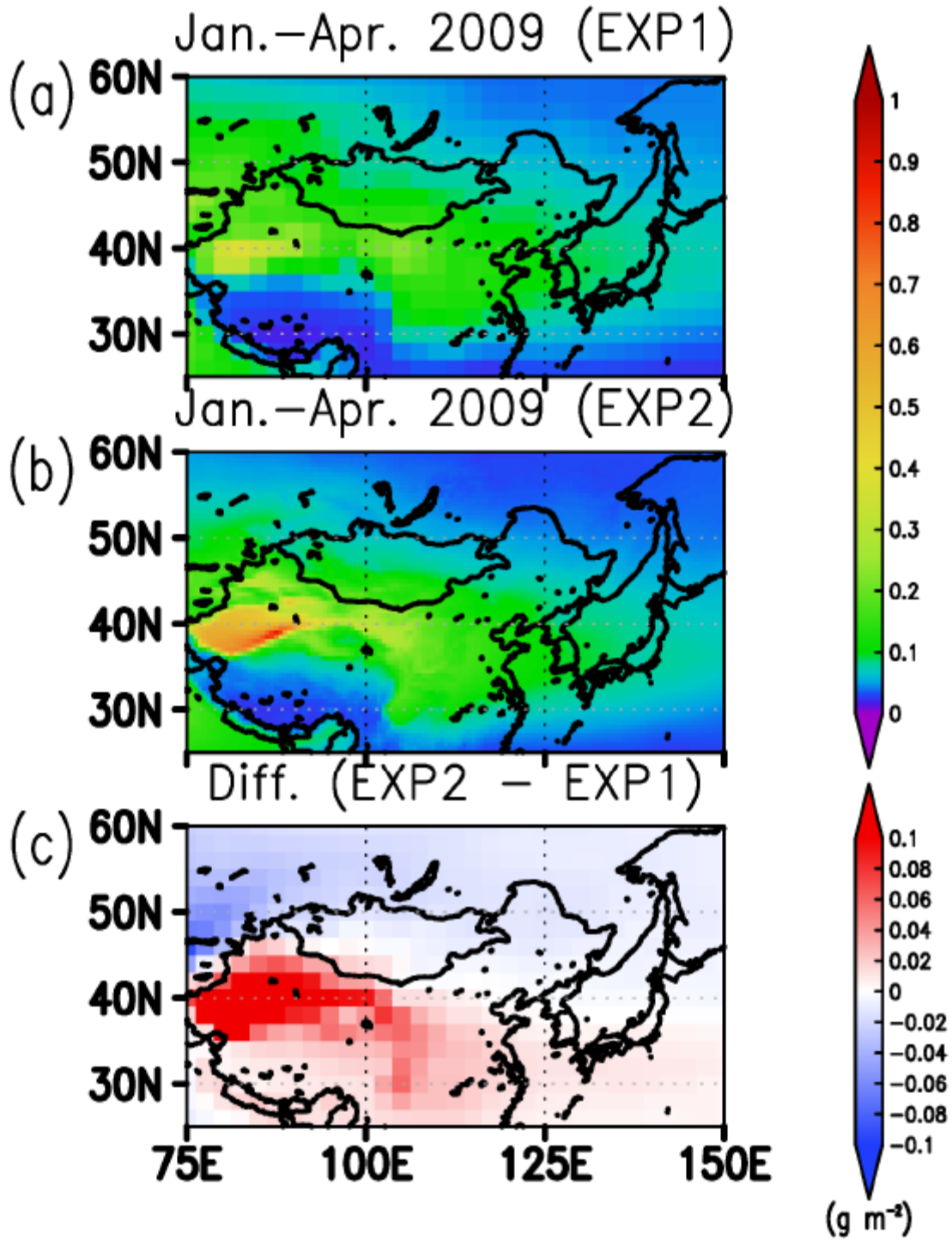


Figure 5

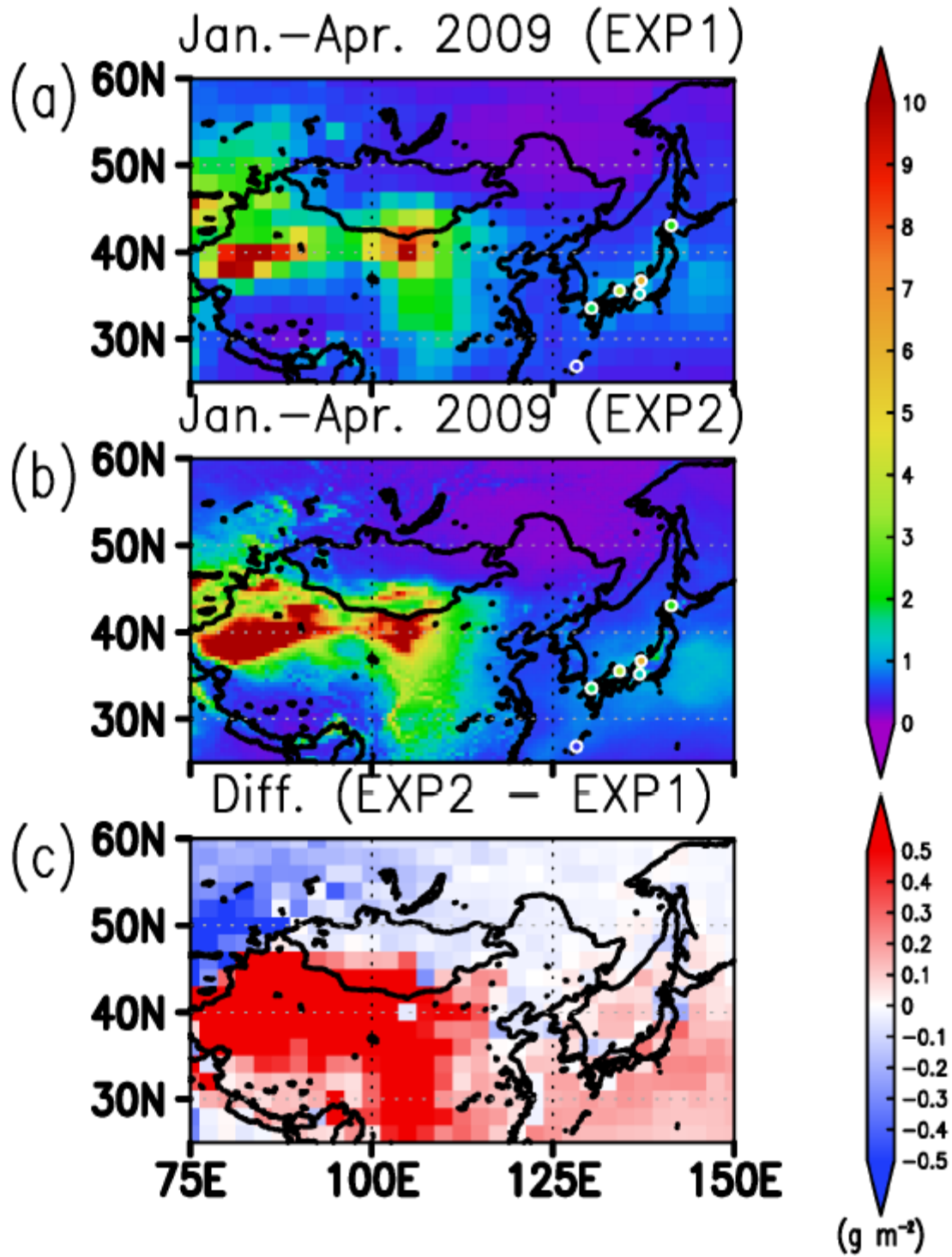


Figure 6

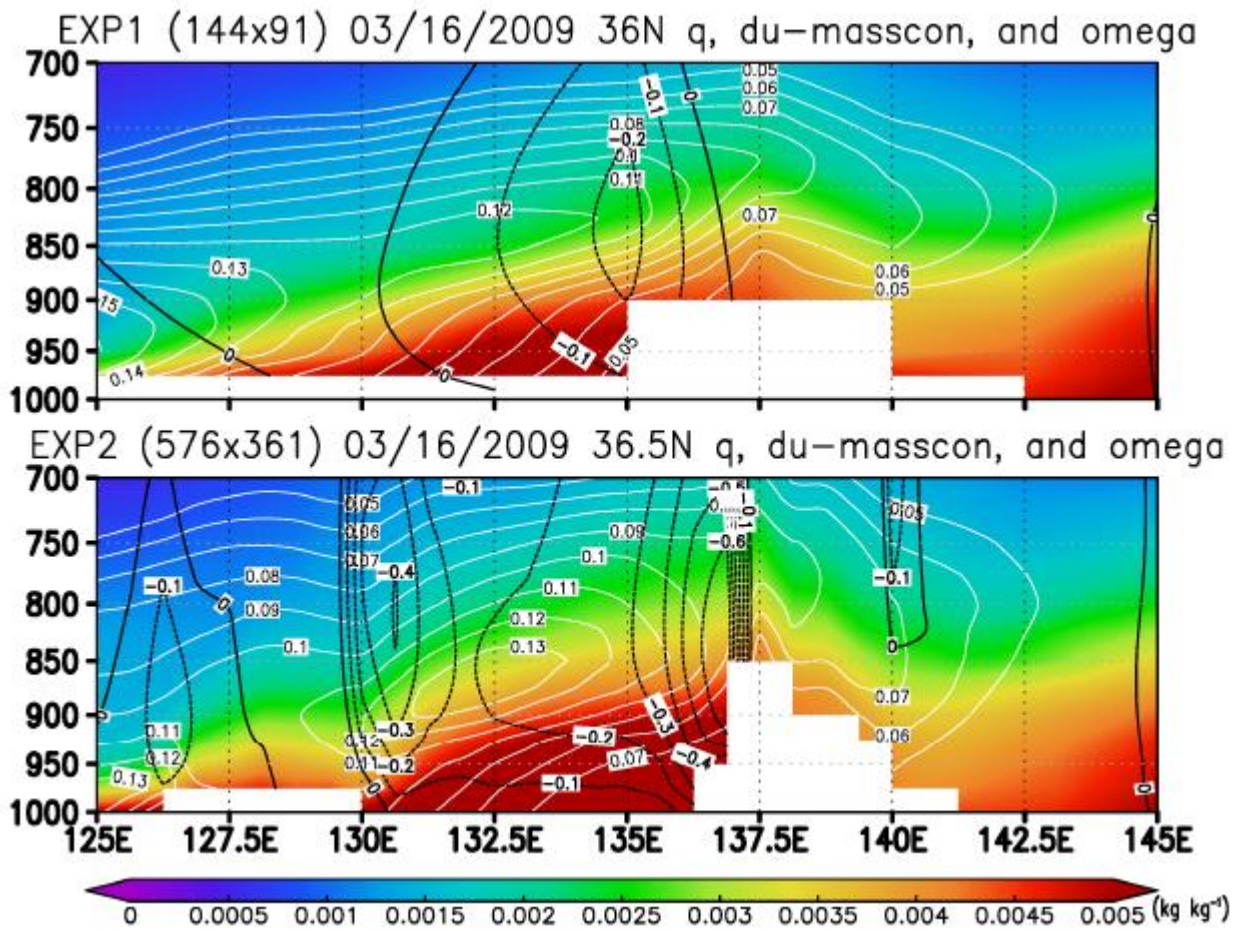


Figure 7

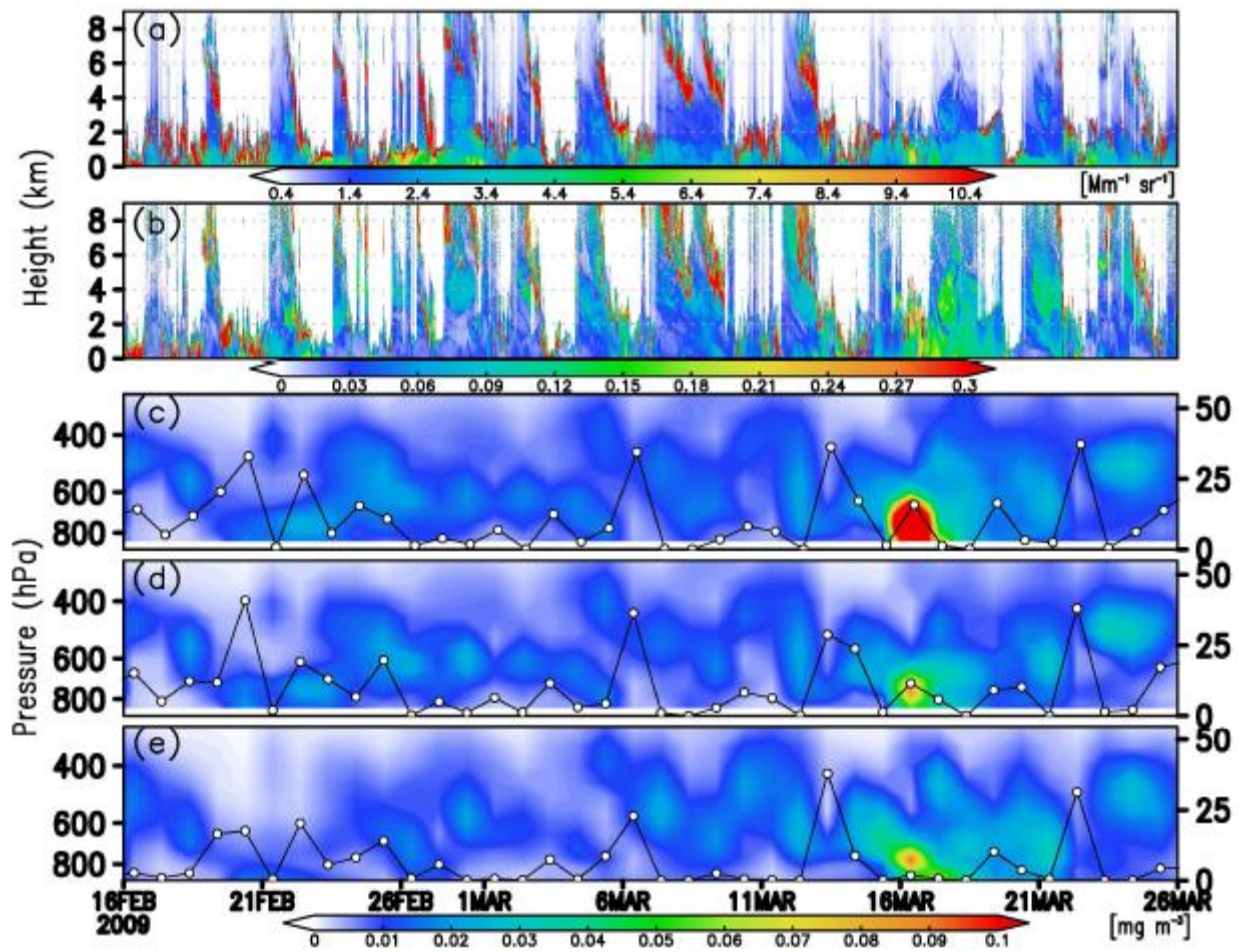


Figure 8

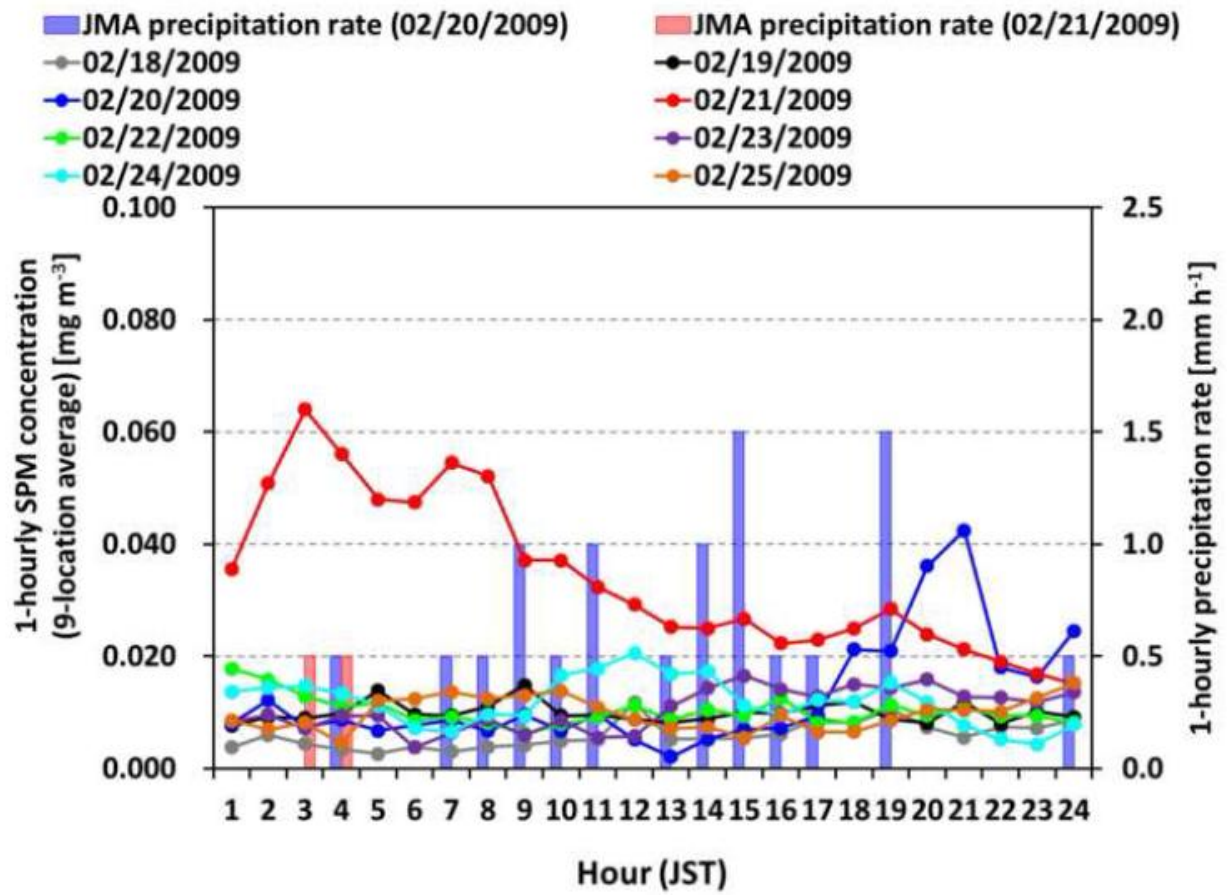


Figure 9

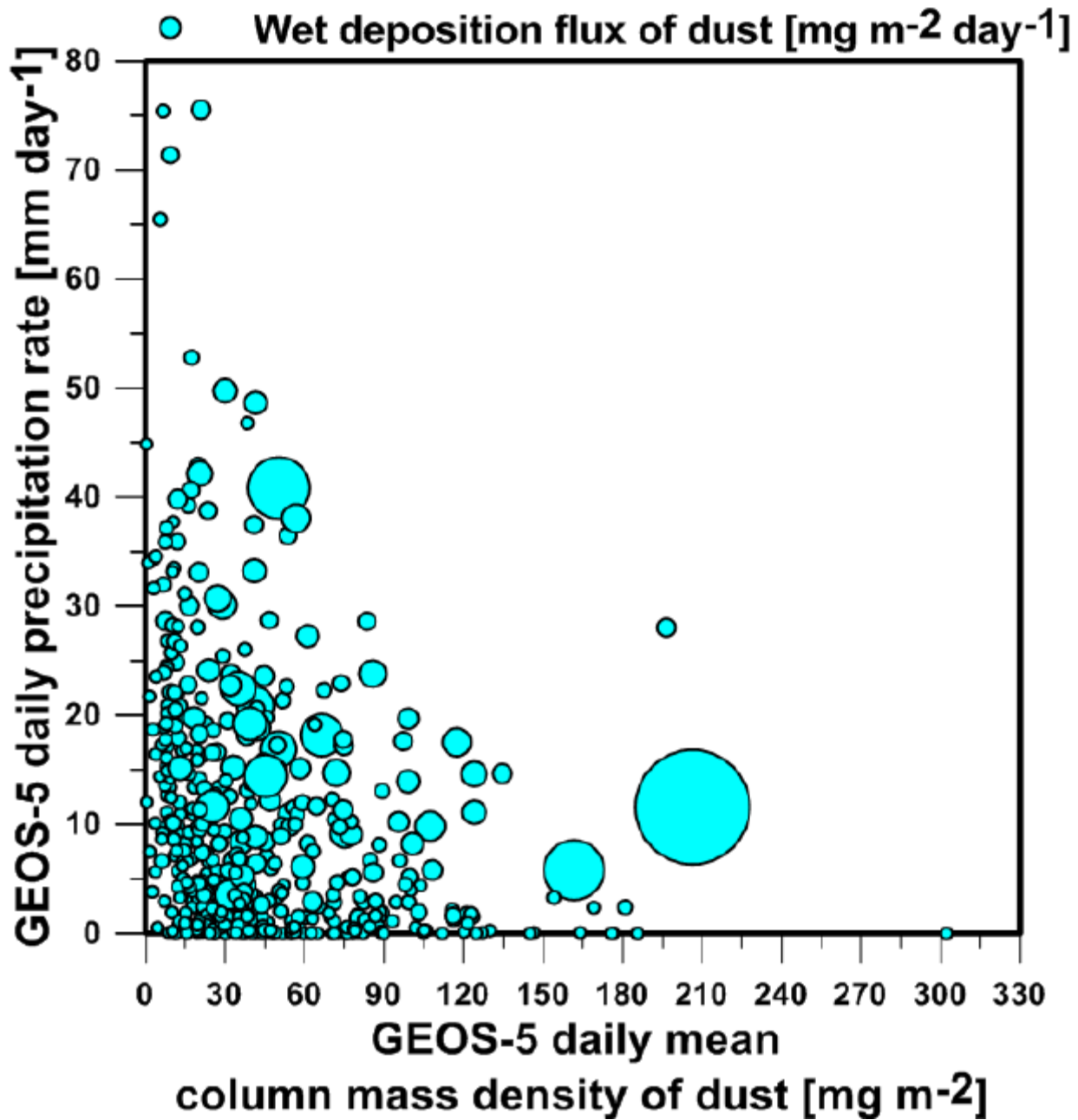


Table 1. Comparisons on the TDP during January-April 2009 at Toyama between the observation by OS11 and the two GEOS-5 experiments (EXP1: 144x91; EXP2: 576x361).

	Dust flux (Obs.)	Dust flux (EXP1)	Dust flux (EXP2)	Dust flux ratio (Obs./EX P1)	Dust flux ratio (Obs./EX P2)	Ratio (EXP1) (wet/total dust)	Ratio (EXP2) (wet/total dust)
2009 Jan.- Apr.	(g m ⁻²)	(g m ⁻²)	(g m ⁻²)				
Toyama	6.1	1.12	2.41	5.44	2.53	0.79	0.93

Note. The observed TDP data during the time period were obtained from Table 1 of OS11. YS14 summarized the similar comparisons but for Sapporo (see their Table S3), and we here summarized the comparisons at Toyama, adapting their table template. In addition notes from YS14 are briefly re-summarized here as follows: The sum of the modeled daily TDP during the time period above is shown in this table; The ratios on "wet/total" are the ratios of the accumulated wet deposition components to the accumulated TDP during the defined precipitation events (see Section 2.1).

Table 2. Comparisons on precipitation during January-April 2009 between the JMA observation at Toyama and two GEOS-5 experiments (EXP1: 144x91; EXP2: 576x361).

	Precip. (JMA Obs.) (mm)	Precip. (EXP1) (mm)	Precip. (EXP2) (mm)	Ratio (JMA Obs./EXP1)	Ratio (JMA Obs./EXP2)
2009 Jan.-Apr. r. Toyama	568	531	1118	1.07	0.51

Note. The JMA-observed precipitation value at Toyama during the OS11 time period above was also summarized in Table 1 of OS11. The table template was adapted from Table S4 of YS14. As also mentioned in SI text of YS14, the threshold value on the defined precipitation event (see Section 2.1) was not applied on the daily precipitation data for the seasonal accumulations here.

Table 3. RMSEs at 6 locations during January-April 2009 between the observed and re-sampled TDPs for each experiment.

Unit: mg m ⁻² day ⁻¹			EXP3	EXP4
	EXP1	EXP2	576x361 + corrected	576x361 MERRA precipitation + aerosol assimilation
Sapporo	21.75	21.15	21.19	20.48
Toyama	99.74	82.08	86.67	63.71
Nagoya	14.83	10.85	11.40	12.54
Tottori	40.15	39.98	40.34	38.61
Fukuoka	11.78	12.50	12.49	10.73
Hedo	5.42	5.86	5.81	6.38

Supplementary Information

Total dust deposition flux during precipitation in Toyama, Japan, in the spring of 2009: A sensitivity analysis with the NASA GEOS-5 Model

Teppe J. Yasunari^{1,2,3}, Peter R. Colarco², William K. M. Lau^{2,4}, Kazuo Osada⁵, Mizuka Kido⁶,
Sarith P. P. Mahanama^{7,2}, Kyu-Myong Kim², and Arlindo M. da Silva²

¹*Goddard Earth Sciences and Technology and Research, Universities Space Research Association, Columbia, MD 21046, USA*

²*NASA Goddard Space Flight Center, Greenbelt, MD 20771, USA*

³*Now at Faculty of Engineering, Hokkaido University, Sapporo, 060-8628, Japan*

⁴*Earth System Science Interdisciplinary Center, University of Maryland, College Park MD 20740, USA*

⁵*Graduate School of Environmental Studies, Nagoya University, Nagoya 464-8601, Japan*

⁶*Toyama Prefectural Environmental Science Research Center, Imizu 939-0363, Japan*

⁷*Science Systems and Applications, Inc., Lanham, MD 20706, USA*

Corresponding author: Tepei J. Yasunari,

Faculty of Engineering, Hokkaido University, Sapporo, 060-8628, Japan.

E-mail: t.j.yasunari@eng.hokudai.ac.jp

1. Additional information on the treatment of the GEOS-5 data

As summarized in Yasunari et al. (2014), (1) the flux (or rate) unit conversion from “per second” to “per day” (i.e., multiplication by 86400 s) was carried out, and (2) daily total precipitation rate was defined as the total amount of convective and large-scale precipitation, and snowfall rates in the unit of $\text{kg m}^{-2} \text{day}^{-1}$ or mm day^{-1} . For EXP4, the surface outputs, such as the surface mass concentration of dust and precipitation rates, were 3-hourly outputs and the daily averaged data were produced from 3-hourly data (i.e., daily mean data; reference time is 12:00 UTC, i.e., 21:00 JST). For the vertical 3D outputs in EXP 4 on dust mass concentration, daily mean outputs were available and used (reference time of 9:00 UTC, i.e., 18:00 JST), which was the same as the daily mean outputs in EXP1-3. The vertical mass concentrations of dust were calculated from the mass mixing ratio with air density data in the daily mean outputs (Figs. 6 and 7). For the calculation of the domain total dust emission amounts in Fig. 3, the areas at each grid point were calculated using the equatorial radius of the Earth of 6378.137 km in the Geodetic Reference System 1980 (GRS80) by Moritz (1980).

2. SPM concentration data in Toyama city

The observed 1-hourly SPM data in Toyama prefecture, which was provided by Toyama Prefectural Environmental Science Research Center (TESC), was used to calculate daily mean data as shown in Fig. S4. If the available 1-hourly data were less than 75% in a day (i.e., less than 18 hours), the daily mean data were not calculated. Instead, it was treated as missing data, at the location, and on that day. In the obtained SPM data, Toyama city has nine locations for the SPM measurement (Table S1). The daily mean SPM data are further averaged within the nine-location data, excluding the missing data

if there were. The nine-location averaged data in Toyama city are considered to be the representative daily mean SPM concentration in Toyama city as shown in Fig. S4. The nine-location averaged daily mean data are further temporally re-sampled with the method mentioned in Section 2.3. Then the accumulated daily mean data with day fraction weights for each sampling time interval at Toyama by Osada et al. (2011; called OS11; Fig. 2 of OS11; Figs. 2a and S2 in this study) or each TSP sample interval (Table S2) was divided by each sampling time interval so as to be the same sampling time intervals of these observations.

3. Comparisons between observed TSP and SPM in Toyama

Fortunately, some sporadic observations of TSP were also available in this study at TESC during March-April 2009 (Table S2). The relationship between the sporadically available TSP and SPM in the observed data was assessed to calculate the estimated TSP from the observed SPM data (i.e., temporally re-sampled nine-location averaged daily mean data). The estimated TSPs were shown in Figs. 2b (in the OS11 sampling interval) and S4 (in daily interval) for the comparisons to the simulated surface mass concentrations of dust in the GEOS-5 experiments (EXP1-4). As mentioned in Section 2.2 in the main text, the information on the difference between SPM and TSP data can provide the information on the mass contributions from the particle size range of larger than 10 μm . Note that the 50% cut-off diameter on SPM measurement is approximately 7 μm (e.g., Fig. 14 of Kasahara, 2002) and some loss of mass during 7-10 μm may be possible in the SPM measurement.

Fig. S3a, shows the comparisons between the observed TSP concentration at TESC and the timely re-sampled mean SPM concentration in Toyama city. Kido et al. (2007) reported that a strong linear

relationship between SPM and TSP concentrations at TESC was found for Asian dust events. Our comparisons also showed a linear relationship (Eq. 1) but its coefficient of determination (R^2) of 0.69 was weaker than that in Kido et al. (2007) ($R^2 = 0.76$; see their Fig. 5). The non-linear relationship (Eq. 2) did show a better R^2 number of 0.80 (Fig. S3a). It can probably be explained by the contributions from not only Asian dust transports but also local background pollution (i.e., non-Asian-dust contributions) to the samples. This is because the observed TSP data shown in Fig. S3 included the time periods of both Asian dust events and non-Asian-dust periods, which were confirmed with the JMA website for Asian dust, Kosa (hereafter called the JMA Kosa website 2009, the same as that in the main text; see the website of JMA available in Japanese: http://www.data.jma.go.jp/gmd/env/kosahp/kosa_table_2009.html). The JMA Kosa website 2009 officially reported Kosa events at Toyama only on March 16-18 in 2009. Based on the results from Kido et al. (2007) and Fig. S3, local pollution and Asian dust may affect the relationships between SPM and TSP differently as shown in Fig. S3a. If so, the non-linear equation (Eq. 2), that includes the non-Asian dust contributions (i.e., more generalized relationship), could explain more about the relationship as shown in Fig. S3a. In fact, the estimated TSP concentrations, which included the non-Kosa periods, with Eq. 2 in Fig. S3a tended to be closer to the observed TSP concentrations at TESC than those estimated with the linear equation by Kido et al. (2007) (Fig. S3b). In addition, the differences between the observed TSP concentrations at TESC and the re-sampled mean observed SPM concentrations in Toyama city were larger for the Asian dust events during March 16-18, when compared to those for the non-Asian-dust time periods (Fig. S3b). In Japan, it has often been observed that transported Asian dust commonly has particle size peaks at around 4 μm (e.g., Nishikawa et al., 1991; Mori et al., 2003).

However, for the Asian dust events, the re-sampled SPM concentration in Toyama city with the particle size of less than 10 μm (i.e., SPM data) explains less than 30% of the observed TSP concentrations at TESC during March 16-19 (Table S3). This indicates that mass contributions of dust from the particle size of more than 10 μm to the TSP concentration were large for the Asian dust events during March 16-18 (Fig. S3b and Table S3). This also suggests that the increase of observed TDP at Toyama (Event C) by OS11 shown in Fig. 2a and S2 was largely contributed by the mass of Asian dust with larger particle size.

4. Asian dust transport contribution to Event B

To discuss whether Event B has Asian dust contributions or not, we further calculated the ensemble backward trajectories using the HYSPLIT model developed by NOAA ARL (Draxler and Rolph, 2014) on their READY website (Rolph, 2014; see the website at: <http://ready.arl.noaa.gov>). The ensemble backward trajectories were calculated for 72-hour backwards from 18:00 UTC February 20 (3:00 JST February 21) from 500 m a.g.l. at Toyama (Fig. S6). The time above corresponds to the peak of the nine-location averaged SPM data in Toyama city from the one-hourly data shown in Fig. 8. The air mass reaching the surface level at Toyama on February 21 included the air mass from around Gobi desert regions. Mizoguchi et al. (2009) discussed the possibilities of detecting Asian dust events at TESC using non-sea-salt calcium ion and lidar data, which included the JMA-reported and non-JMA-reported Asian dust events. In their study, the daily mean SPM concentrations observed at TESC on their six Kosa judgement days (these were non-JMA-reported Kosa events, but possibly judged as Kosa days based on their method) were in the range of 0.0262-0.0382 mg m^{-3} as shown in their Table 1. The daily mean

SPM concentration on February 21, when averaging all nine locations in Toyama city (Fig. S4), was 0.0340 mg m^{-3} and within the range above in Mizoguchi et al. (2009) on the Kosa judgement days. Matoba et al. (2005) also mentioned that SPM measurement could be used to detect Asian dust events including weak events, together with pressure pattern and backward trajectory analyses, even though JMA officially did not detect Asian dust events. Considering all the above, the SPM increase in Toyama on February 21 shown in Fig. 8 could be judged as a weak Kosa case that was not reported by the JMA observation (see the JMA Kosa website 2009). In conclusion, the increases of the observed SPM (or estimated TSP) concentration in Toyama city (Figs. S4 and 8) and of the lidar signals near the surface (Figs. 7a-b) at TESC on February 21 were probably due to weak Asian dust transport from around the Gobi desert.

References

- Draxler, R. R., Rolph, G. D., 2014. HYSPLIT (HYbrid Single-Particle Lagrangian Integrated Trajectory) Model access via NOAA ARL READY Website (<http://ready.arl.noaa.gov/HYSPLIT.php>). NOAA Air Resources Laboratory, Silver Spring, MD.
- Kasahara, M., 2002. The present state and future assignments of air pollution by particulate matter—The meaning of innovation of PM_{2.5}—. *J. Jpn. Soc. Atmos. Environ.*, 37(2), 96-107, doi:10.11298/taiki1995.37.96 (in Japanese with English abstract).
- Kido, M., Nakamura T., Yamazaki, T., Mizoguchi, T., Kondo, T., Toriyama S., Hashimoto, J., Kawasaki, K., 2007. Study on atmospheric deposition in East Asia (the first report)— Concentration of chemical constituents in atmospheric aerosol particles during Kosa events in Toyama—. Annual Report of Toyama Prefectural Environmental Science Research Center, 35, 69-75 (in Japanese).
- Matoba, S., Mori, I., Hayakari, S., Nishikawa, M., 2005. New method of detecting Kosa (Asian dust) from SPM data measured by environmental air monitoring stations. *J. Aerosol Res. (Earozeru Kenkyu)*, 20(3), 225-230, doi:10.11203/jar.20.225 (in Japanese with English abstract).
- Mizoguchi, T., Kawasaki, K., Shimizu, A., Satake, H., 2009. Investigation of dry deposition in Toyama and analysis by rider during the period of high SPM concentration. *J. Jpn. Soc. Atmos. Environ.*, 44(3), 155-165, 2009, doi:10.11298/taiki.44.155 (in Japanese with English abstract; note that “rider” for the original title above should be “lidar” but we put the title as it was for this reference).
- Mori, I., Nishikawa, M., Tanimura, T., Quan H., 2003. Change in size distribution and chemical composition of kosa (Asian dust) aerosol during long-range transport. *Atmos. Environ.*, 37(30), 4253-4263, doi:10.1016/S1352-2310(03)00535-1.

- Moritz, H., 1980. Geodetic reference system 1980. Bull. Geod., 54(3), 395-405, doi: 10.1007/BF02521480.
- Nishikawa, M., Kanamori, S., Kanamori, N., Mizoguchi, T., 1991. Ion equivalent balance in water soluble constituents of Kosa aerosol. Earozoru Kenkyu, 6(2), 157-164, doi:10.11203/jar.6.157 (in Japanese with English abstract).
- Osada, K., Ura, S., Kagawa, M., Mikami, M., Tanaka, T. Y., Matoba, S., Aoki, K., Shinoda, M., Kurosaki, Y., Hayashi, M., Shimizu, A., Uematsu, M., 2011. Temporal and spatial variations of wet deposition flux of mineral dust in Japan. SOLA, 7, 49-52, doi:10.2151/sola.2011-013.
- Rolph, G. D., 2014. Real-time Environmental Applications and Display sYstem (READY) Website (<http://ready.arl.noaa.gov>). NOAA Air Resources Laboratory, Silver Spring, MD.
- Yasunari, T. J., Lau, K.-M., Mahanama, S. P. P., Colarco, P. R., da Silva, A. M., Aoki, T., Aoki, K., Muraio, N., Yamagata, S., Kodama, Y., 2014. Goddard SnoW Impurity Module (GOSWIM) for the NASA GEOS-5 Earth System Model: Preliminary comparisons with observations in Sapporo, Japan. SOLA, 10, 50-56, doi:10.2151/sola.2014-011.

Table S1. Locations for the SPM observations in Toyama city.

Location name	Location ID	lon.	lat.
Toyama Shibazono	16201021	137.20333	36.69472
Toyama Shinmei	16201100	137.18472	36.68694
Toyama Mizuhashi	16201110	137.30472	36.74972
Toyama Ninagawa	16201140	137.22139	36.65500
Toyama Iwase	16201400	137.23194	36.74194
Toyama Jyoushi	16201510	137.21222	36.69222
Toyama Toyota	16201520	137.23639	36.72389
Fuchu Hayahoshi	16362010	137.15194	36.66028
Fuchu Tajima	16362510	137.17667	36.67194

Note. The location information was provided by TESC.

Table S2. Sampling time period for TSP observations at TESC.

Sampling start time	Sampling end time
2009/3/16 13:08	2009/3/17 10:37
2009/3/17 11:00	2009/3/18 10:30
2009/3/18 11:00	2009/3/19 11:00
2009/3/19 11:04	2009/3/20 10:54
2009/4/6 9:07	2009/4/7 9:05
2009/4/21 17:40	2009/4/23 8:23
2009/4/25 13:00	2009/4/27 8:28

Table S3. Ratios of the re-sampled mean SPM to the observed TSP concentrations in 2009.

TSP sampling dates	Ratio (re-sampled SPM/observed TSP)
March 16-17	0.201
March 17-18	0.255
March 18-19	0.237
March 19-20	0.372
April 6-7	0.629
April 21-23	0.343
April 25-27	0.735

Note. The re-sampled mean SPM and the observed TSP concentration data were plotted in Fig. S3.

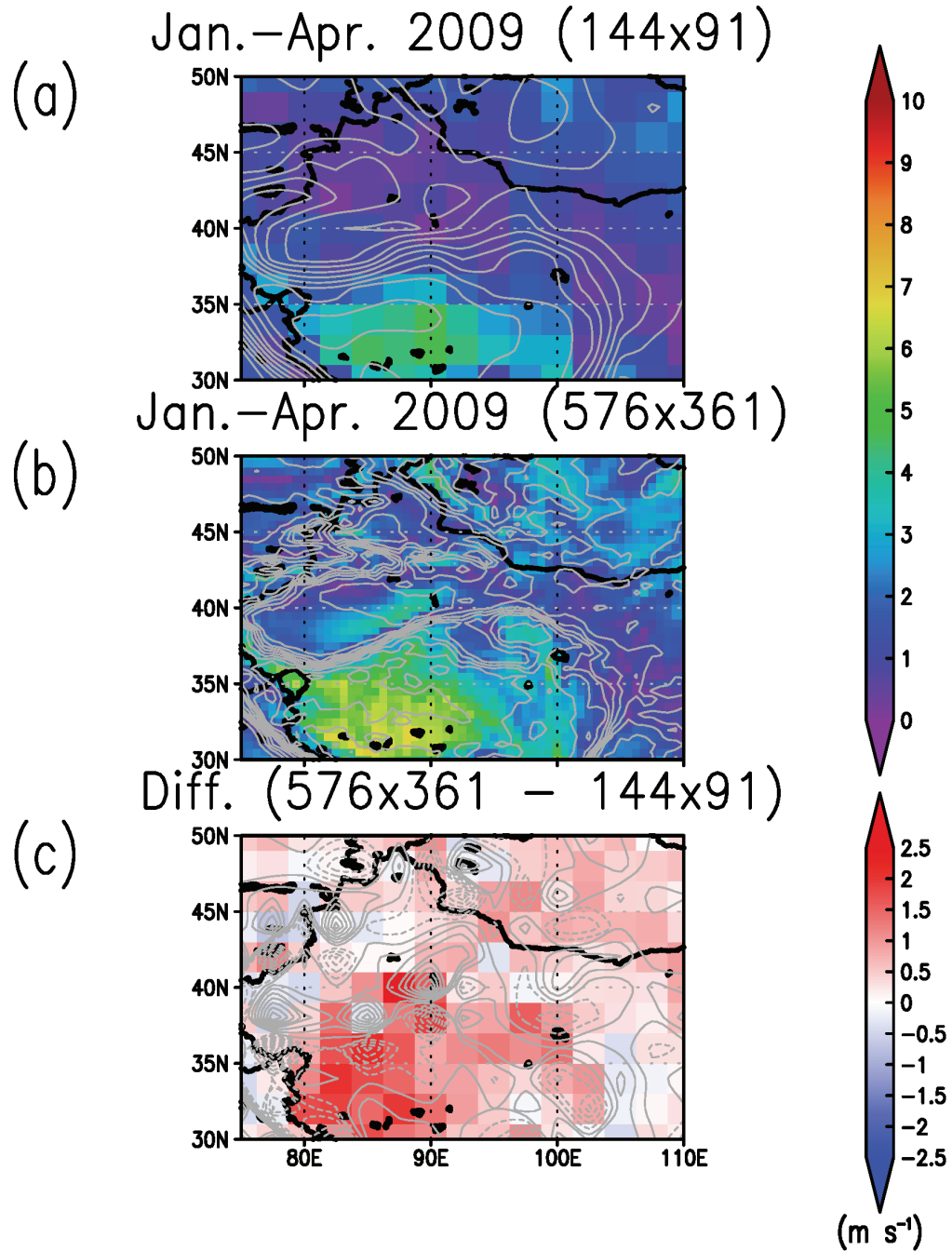


Fig. S1. Surface geopotential height (contours in gray with interval of 500 m) and mean horizontal wind velocity at 10 m in January – April in 2009 by the GEOS-5 experiments (grid-filled in rainbow colors) near the dust source regions in East Asia with two different horizontal resolutions (a: EXP1; b: EXP2) and its difference (c: EXP2 minus EXP1; wind velocity: grid-filled from blue to red; surface geopotential height: contours in gray with interval of 10 m). In Panel (c), the solid and dashed contours denote positive and negative differences, respectively. For the difference, the data from EXP2 were re-gridded into the same horizontal resolution of EXP1.

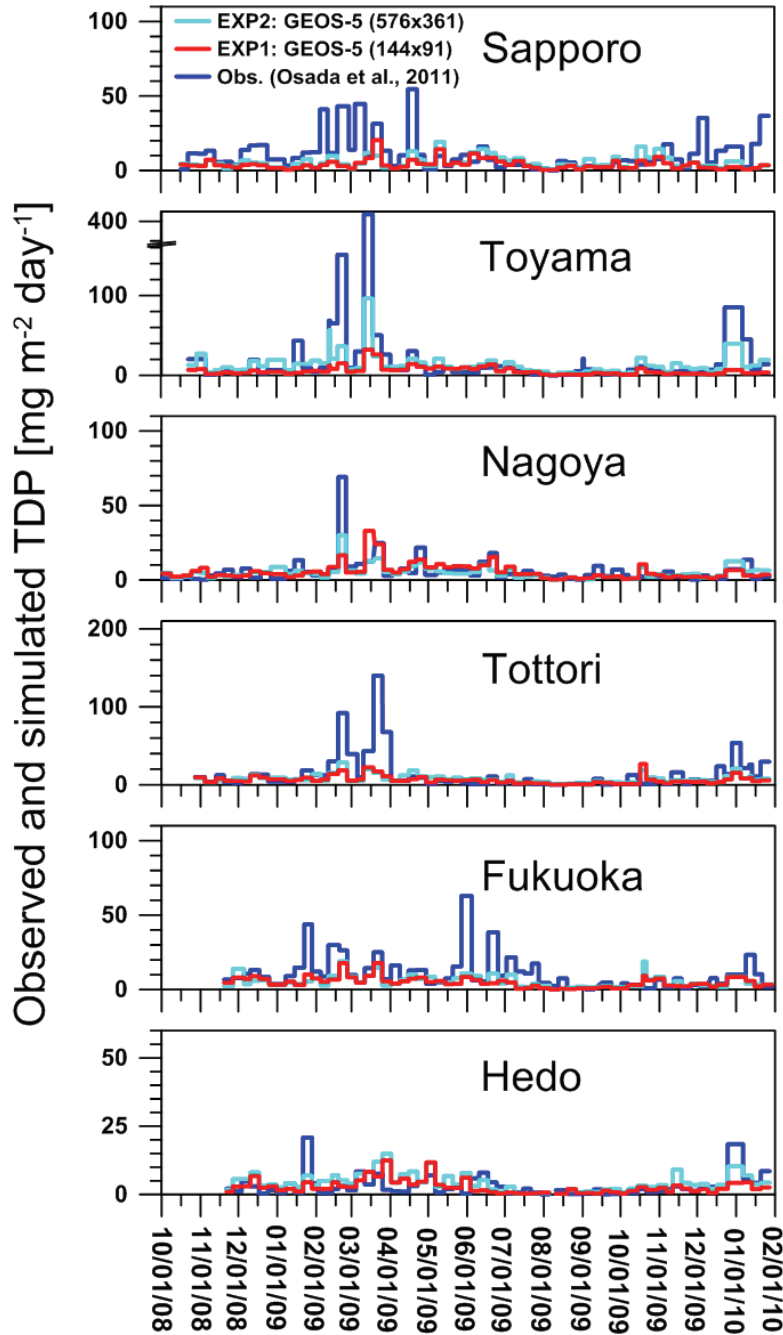


Fig. S2. Comparisons between temporally re-sampled TDP modeled by GEOS-5 (EXP1 in red and EXP2 in light blue) and observed TDP (blue; the data obtained from Fig. 2 of OS11) at 6 locations in Japan. Break axis was used for Toyama. From one sampling time to the next, there were often slight time lags but we continuously plotted between sampling times. For the time period when the sampling time was not fully within the time period during October 2008 and January 2010, the data were not used for plotting at each location. The daily GEOS-5 data at Toyama and Nagoya from EXP1 were the same because these locations were in the same grid point in EXP1 as seen in Fig. 1. During August 6-9 in 2009, no observation at Hedo was available due to a typhoon.

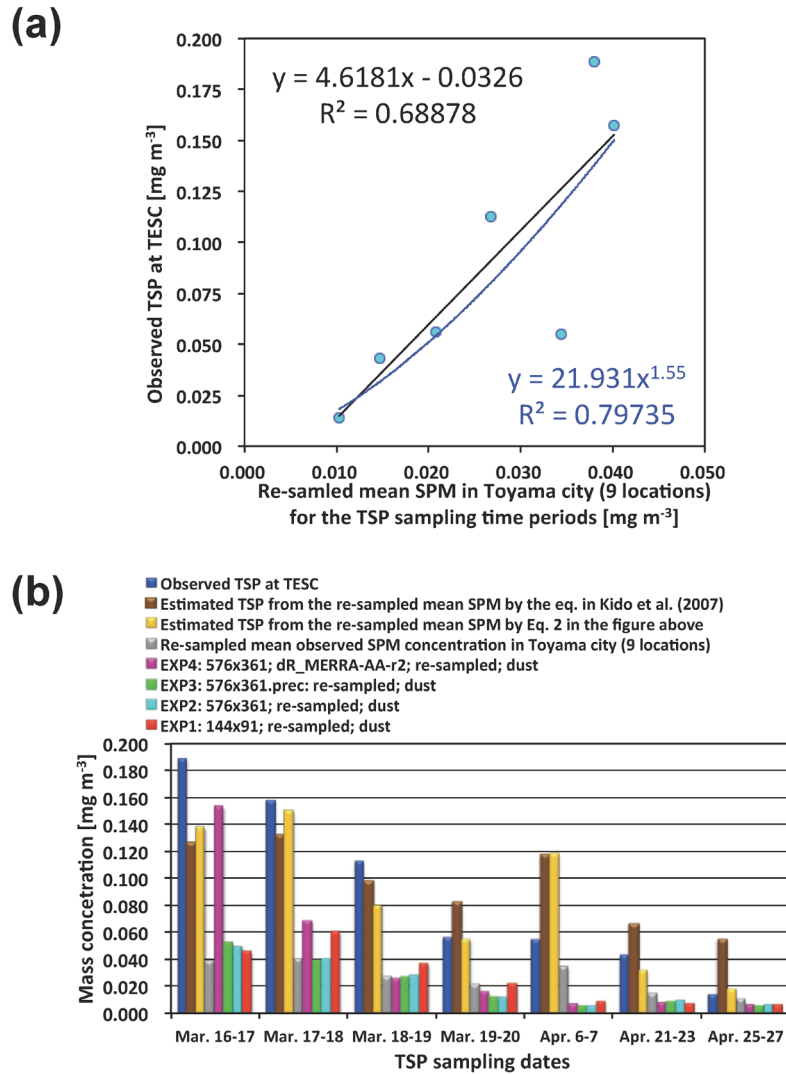


Fig. S3. Comparisons among observed TSP concentrations at TESC, temporally re-sampled mean observed SPM concentration in Toyama city, estimated TSP from the SPM data, and temporally re-sampled surface mass concentration of dust from the GEOS-5 experiments at the OS11 Toyama site. (a) A relationships between the observed TSP concentrations at TESC and temporally re-sampled mean observed SPM concentrations in Toyama city (averaging nine locations), which are also shown in Fig. S3b. Two types of regression equations (Eq.1: linear; Eq. 2: non-linear) are applied here. (b) Comparisons among the data for the time periods when seven TSP samplings were carried out. The temporally re-sampled data here are for the time periods shown in Table S2. Two estimated TSP data are shown in Panel (b) based on the temporally re-sampled mean SPM data with Eq. 2 in Panel (a) and the equation of Kido et al. (2007) (see their Fig. 5). On March 16-18, Asian dust events were officially observed in Toyama by JMA (see the JMA Kosa website 2009).

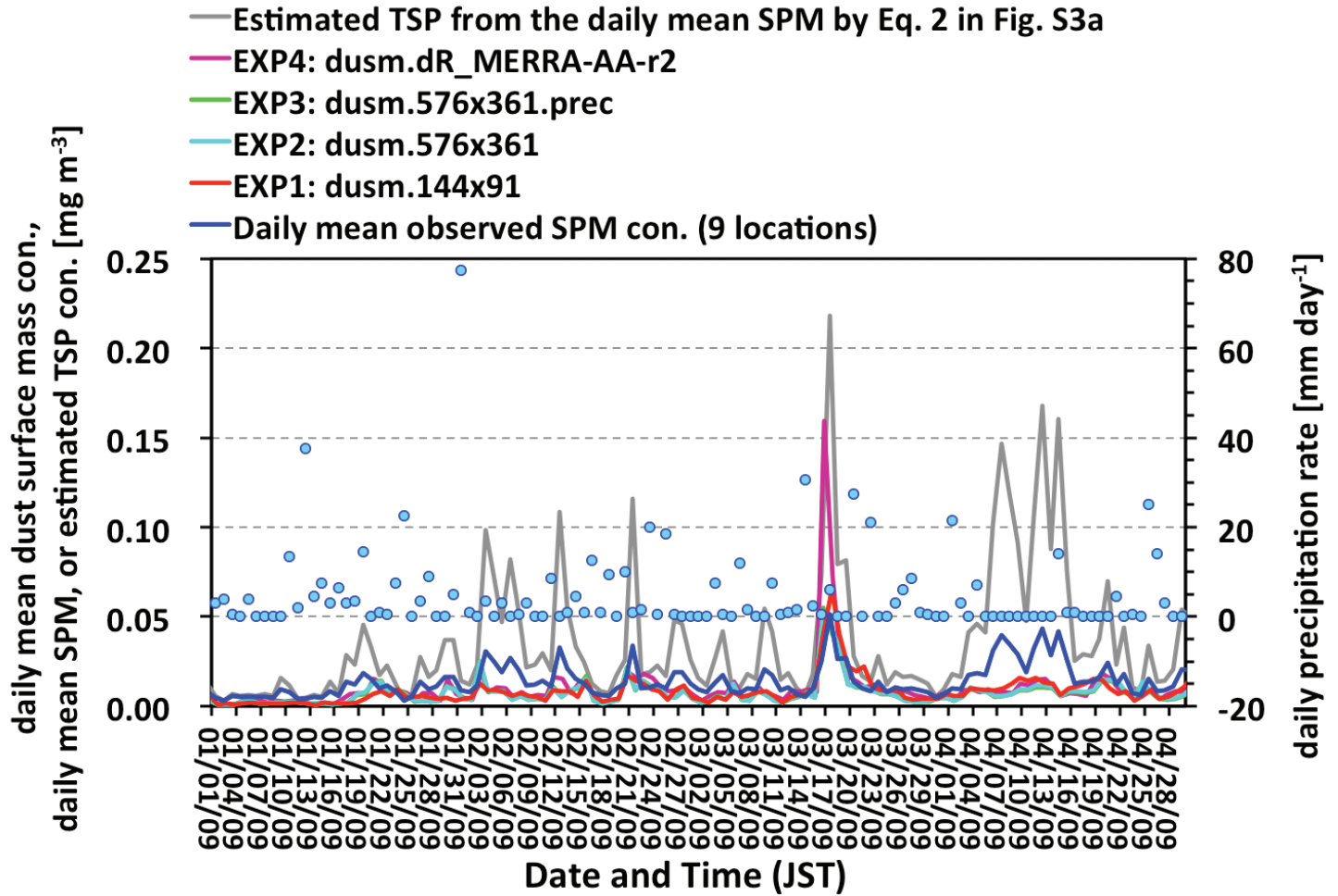


Fig. S4. Similar to Fig. 2b but, instead, indicates “daily” data in Toyama during January – April 2009 on the simulated daily mean surface mass concentration of dust by GEOS-5 (EXP1-4), daily mean observed SPM concentration (i.e., based on the original 1-hourly data provided by TESC; averaged among nine locations in Toyama city; also see SI text), and JMA-observed daily precipitation rate (see the JMA website in the main text). The TSP concentration was “estimated” with Eq. 2 in Fig. S3a with the SPM data. Reference time for the plots of EXP1-3, EXP4, SPM (or estimated TSP), JMA precipitation data is 18:00, 21:00, 12:00, and 12:00 JST, respectively. To make it easier to see, the scale on the right side for the JMA observed daily precipitation rate starts from $-20.0 \text{ mm day}^{-1}$.

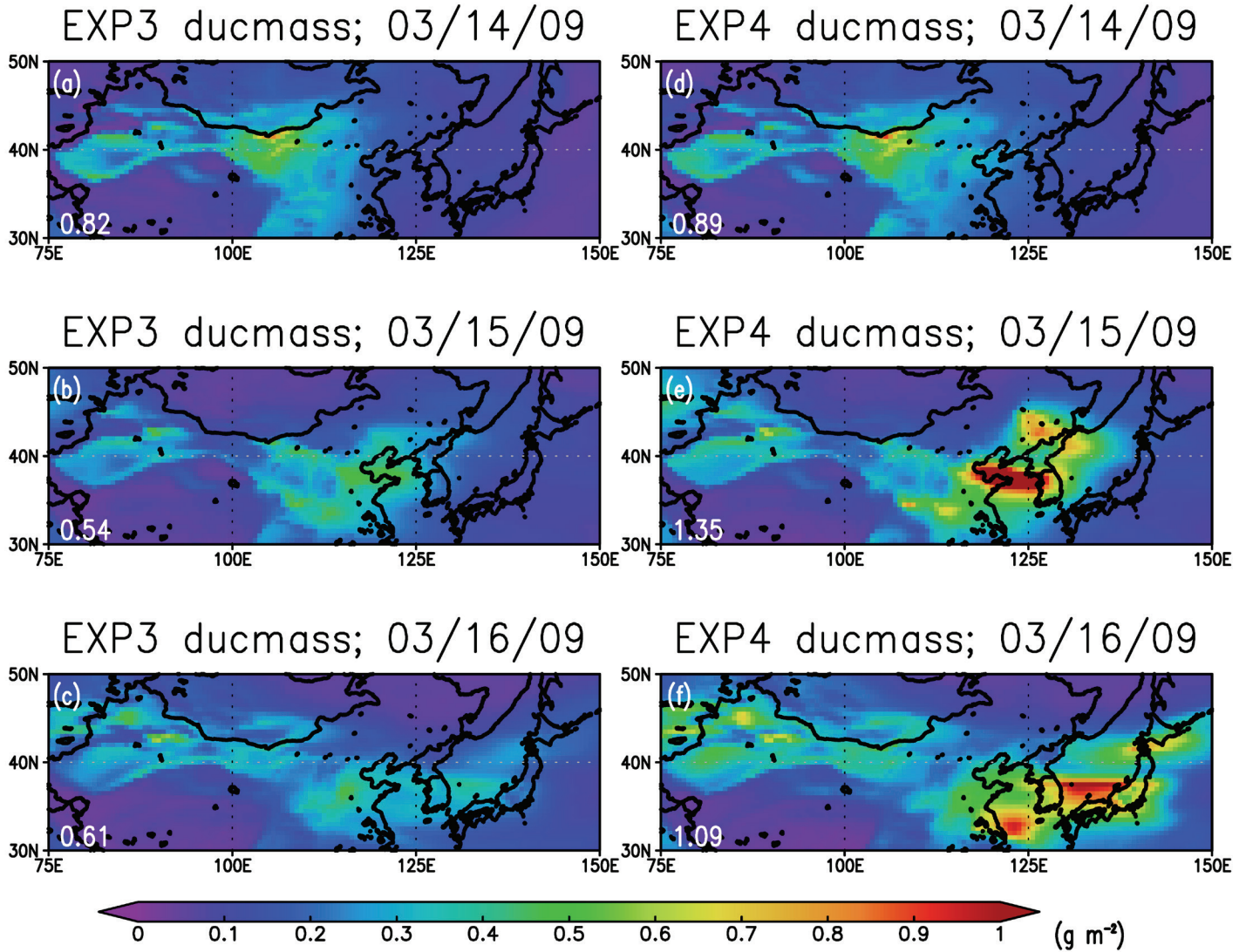


Fig. S5. Day-by-day migration of column mass density of dust during March 14-16, 2009, over East Asia for Event C in EXP3 (a: March 14; b: March 15; c: March 16; the reference time of the daily mean output is 9:00 UTC) and in EXP4 (d: March 14; e: March 15; f: March 16; the reference time of the calculated daily mean data from 3-hourly outputs is 12:00 UTC; see Section 1 of SI on the daily mean data in EXP4). The values shown in each panel are the maximum numbers within the domain in each panel.

NOAA HYSPLIT MODEL
 Backward trajectories ending at 1800 UTC 20 Feb 09
 GDAS Meteorological Data

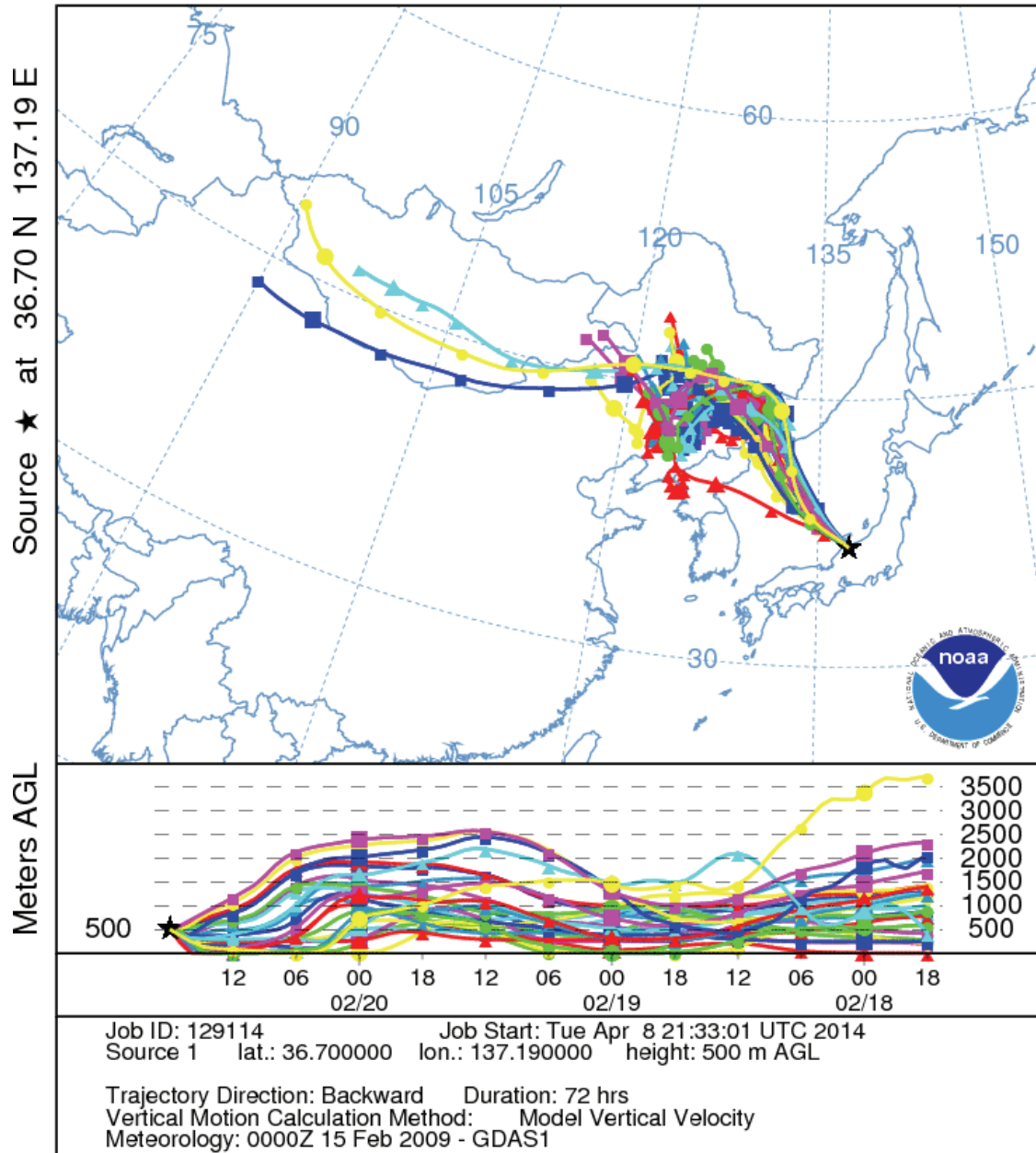


Fig. S6. Ensemble backward trajectories for 72-hour period simulated by the HYSPLIT model (Draxler and Rolph, 2014) in NOAA ARL available on their READY website (Rolph, 2014; see the website a: <http://ready.arl.noaa.gov>) from the OS11 Toyama location (500 m a.g.l) for Event B, starting at 18:00 UTC on February 20, 2009 (i.e., 3:00 JST February 2009, corresponding to the timing of the SPM peak shown in Fig. 8).

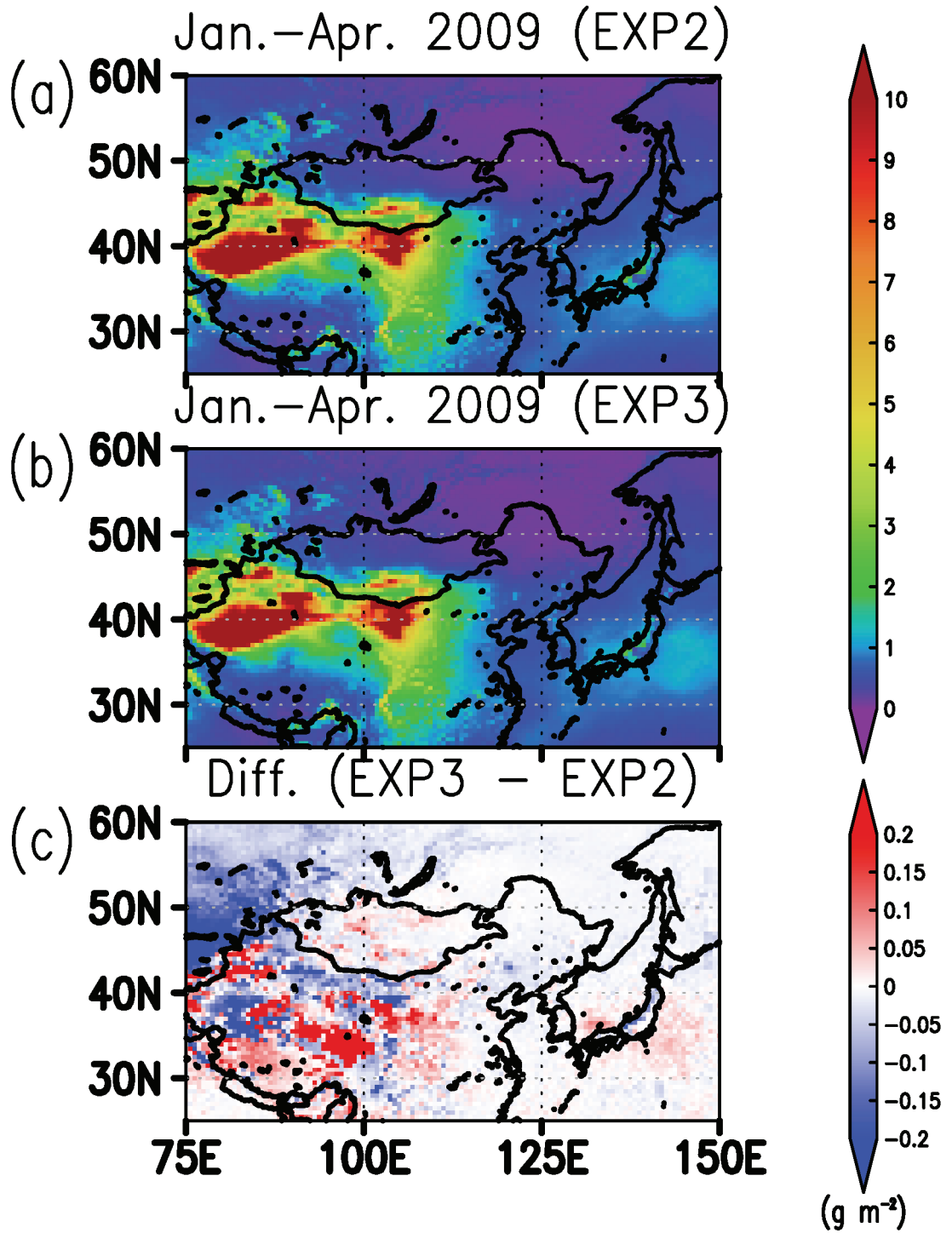


Fig. S7. Similar to Fig. 5 (i.e., TDP in EXP1 and EXP2) but, instead, indicates TDP in (a) EXP2, (b) EXP3, and (c) the difference between EXP2 and EXP3 (EXP3 minus EXP2).